Phosphatidylethanolamine produced in the inner mitochondrial membrane is essential for yeast cytochrome bc_1 complex function

Elizabeth Calzada[1] and Steven M. Claypool[1]

From the [1] Department of Physiology, Johns Hopkins University School of Medicine, Baltimore, MD, USA

To whom correspondence should be addressed: Steven M Claypool, Dept. of Physiology, Johns Hopkins School of Medicine, 725 N. Wolfe St., Baltimore, MD 2125-2185. Tel. (410) 614-1786; Fax. (410) 955-0461; E-mail: sclaypo1@jhmi.edu

ABBREVIATIONS:

Cardiolipin (CL), Cytochrome bc_1 complex (complex III), cytochrome oxidase (complex IV), Coenzyme Q (CoQ), diacylglycerol (DAG), endoplasmic reticulum (ER), inner membrane (IM), intermembrane space (IMS), *m*-chlorophenyl hydrazine (CCCP), mitochondrial-associated membrane (MAM), mitochondrial contact site and cristae organizing system (MICOS), mitochondrial DNA (mtDNA), *n*-Dodecyl-β-D-maltoside (DDM), outer membrane (OM), oxidative phosphorylation (OXPHOS), phosphatidic acid (PA), phosphatidylcholine (PC), phosphatidylethanolamine (PE),phosphatidylinositol (PI), phosphatidylserine (PS), phosphatidylserine decarboxylase 1 (Psd1), respiratory control ratio (RCR), synthetic complete dextrose (SCD), synthetic complete lactate (SC-LAC), synthetic complete ethanol glycerol (SCEG), tetramethyl-*p*-phenyldiamine (TMPD), wildtype (WT)

ABSTRACT:

The capacity of mitochondria to produce ATP is linked with its ability to generate phosphatidylethanolamine (PE). Of the four separate PE biosynthetic pathways in eukaryotes, three reside in the endoplasmic reticulum (ER) and one occurs in the inner membrane (IM) of mitochondria and is executed by phosphatidylserine (PS) decarboxylase (Psd1p). Deletion of Psd1 is lethal in mice and disrupts mitochondrial morphology, impairs cell growth, and diminishes respiratory capacity in both yeast and mammalian cells. This implies that the ER pathways for PE biosynthesis are unable to compensate for the absence of Psd1. We hypothesize that this failure is due to the inefficient trafficking of extra-mitochondrial PE into the IM. Here, we sought to determine which aqueous compartment, the cytosol or the mitochondrial intermembrane space, is the greatest barrier for PE trafficking to the IM. Yeast strains expressing two novel chimeric constructs that re-direct Psd1p to either the outer mitochondrial membrane (OM-Psd1p) or the endomembrane system (ER-Psd1p) were characterized. By comparing growth phenotypes, phospholipid turnover, and the activities of electron transport chain complexes of these PE re-routed strains, we identified the intermembrane space as the greatest barrier for PE import. Interestingly, PE made outside of the IM was able to rescue the activity of respiratory complex IV but not complex III. Since the activity of both complexes is dependent on PE, this suggests that Psd1p and/or PE made in the IM is uniquely able to support complex III function.

INTRODUCTION:

The evolutionary design of living cells has revealed redundancies in various metabolic pathways to promote survival. Importantly however, the sequestration of enzymes and their substrates into different membrane compartments allows for the enrichment and regulation of

metabolite synthesis in regions of the cell where they are essential. Such is the case for the biosynthesis of the abundant membrane phospholipid, phosphatidylethanolamine (PE). In mammalian cells PE is synthesized by four separate pathways, three of which localize to the endoplasmic reticulum (1). A final pathway is dependent on phosphatidylserine decarboxylase (Psd1p) which is spatially isolated within the mitochondrial inner membrane (IM) (2-5). The predominant pathways for PE production include the Kennedy pathway, which synthesizes PE through the stepwise conjugation of CDP-ethanolamine to diacylglycerol (DAG) and the Psd pathway which utilizes phosphatidylserine (PS) as a substrate to generate PE (1). In multicellular organisms, preference for either the Kennedy pathway or the Psd pathway varies between tissues and cell types (6). Notably, deletion of either pathway is lethal during murine embryogenesis, highlighting the importance of PE generation in both the ER and mitochondrial compartments for development (7, 8).

Conservation of the Psd pathway from bacteria to humans likely reflects the endosymbiotic origin of mitochondria which in turn suggests that mitochondrial PS and PE metabolism has been preserved to optimize mitochondrial performance (6). Indeed, deletion of phosphatidylserine decarboxylase (*Pisd* in mouse and humans and *PSD1* in yeast) in eukaryotic cells decreases cellular growth, impairs oxidative phosphorylation, produces aberrant mitochondrial morphology, and diminishes PE levels in cells and mitochondria (7, 9-12). The Psd pathway is the predominant pathway for PE production in *Saccharomyces cerevisiae* and produces up to 70% of cellular PE in the cell (13). In contrast to mammals, yeast additionally contain Psd2p which localizes to either Golgi or endosomal compartments (5, 14). Deletion of *PSD2* alone does not recapitulate any of the mitochondrial defects associated with loss of *PSD1*, further emphasizing the importance of the mitochondrial PE biosynthetic pathway therein (5). The combined absence of *PSD1* and *PSD2*

68 produces a strain that is auxotrophic for exogenous ethanolamine which is used to generate PE
69 through the Kennedy pathway. As the severity of PE depletion can be genetically and
70 metabolically adjusted in yeast, this organism has served as an efficient model for studying the
71 importance of the mitochondrial Psd pathway for cellular respiration.

72 To our knowledge, characterization of the Psd pathway over the last 50 years of research
73 has revealed detailed mechanistic insight into the biogenesis of the mature Psd1p enzyme (15). In
74 yeast, *PSD1* is a nuclear encoded gene whose transcript is translated on cytosolic ribosomes which
75 produce a full-length zymogen that is catalytically inactive. Upon its mitochondrial import, two
76 matrix metalloproteases sequentially process the N-terminus of Psd1p which then undergoes a
77 third processing event that is executed internally by the enzyme itself at the conserved C-terminal
78 LGST motif (2, 3). This unique autocatalytic processing event severs Psd1p into the large
79 membrane-anchored β subunit and the small α subunit and is performed by a self-contained
80 catalytic triad typical of serine proteases (16, 17). Self-processing endows the small α subunit with
81 an N-terminal pyruvoyl prosthetic group that is crucial for its decarboxylase activity. Post-
82 cleavage, the two Psd1p subunits remain non-covalently associated within the inner membrane
83 where they decarboxylate PS to PE (17).

84 The substrate of Psd1p, PS, is synthesized on the mitochondrial-associated membrane
85 (MAM) of the ER (18). Thus, the amphipathic PS must be imported from the ER and traverse
86 through two aqueous compartments, the cytosol and the mitochondrial intermembrane space
87 (IMS), to reach Psd1p at the IM (19). Although the specific role played by ER-mitochondria
88 membrane tethers in PS import remains elusive (20-24), recent evidence in yeast implicates that
89 Mic60p, a subunit of the mitochondrial contact site and cristae organizing system (MICOS) works
90 in conjunction with the soluble lipid carrier, Ups2p, to expose PS for Psd1p decarboxylation (25,

26). Whether or not a parallel pathway exists for PE import into the IM remains unclear. The lethal consequence of *pisd* deletion in mice and the failure of supplemental ethanolamine to rescue the respiratory defects of *psd1*Δ yeast were taken as evidence that PE made outside of the mitochondrion is unable to compensate for the absence of Psd1p (1, 7, 11, 27). However, it was recently reported that PE made by the Kennedy pathway can in fact restore the impaired oxidative phosphorylation of *psd1*Δ yeast suggesting that extra-mitochondrial PE can partially compensate for the absence of the Psd pathway (28).

Here, we sought to define which aqueous compartment is a barrier for PE trafficking into the mitochondrion in *S. cerevisiae.* Previously, we generated a chimeric Psd1p protein, ER-Psd1p, which is targeted to the endosomal compartment by switching the mitochondrial targeting sequence of Psd1p with the signal sequence of carboxypeptidase Y (29, 30). In the current study, we further characterized the cell biology of ER-Psd1 yeast, together with an OM-targeted chimeric Psd1p (OM-Psd1p), to test if the cytosol, IMS, or both, are barriers that prevent non-mitochondrially produced PE from functionally rescuing the absence of PE made in the IM. Alongside strains expressing these re-directed Psd1p constructs, we compared the mitochondrial function of *psd1*Δ*psd2*Δ yeast grown in the non-fermentable carbon source, lactate, with or without exogenous ethanolamine supplementation, to evaluate the ability of the Kennedy pathway to support mitochondrial function. Intriguingly, in contrast to cytochrome *c* oxidase (complex IV), cytochrome bc_1 respiratory complex (complex III) activity was impaired in the absence of IM-synthesized PE even after supplementation with ethanolamine. This indicates that the IMS is the greatest obstacle for extra-mitochondrially produced PE to reach the IM where it is crucial for complex III function. Our results demonstrate that Psd1p and/or PE made in the IM by Psd1p is critical to support full complex III function.

RESULTS

The impaired respiratory growth of psd1Δ yeast is not rescued by PE synthesis through the Kennedy pathway

The ability of supplemental ethanolamine to rescue to the respiratory growth defect of *psd1*Δ yeast has been reported by some groups (28) but not others (1, 11, 27). Thus, this is an important controversy to resolve. If extra-mitochondrially produced PE can replace PE normally made in the IM, then this would imply that the mitochondrial Psd1 pathway *per se*, is not necessary for mitochondrial function. By extension, it would suggest that mechanisms to move extra-mitochondrially produced PE into mitochondria are robust enough to compensate for the absence of Psd1p. Therefore, we tested the growth of wildtype (WT), *psd1*Δ, *psd2*Δ*,* and *psd1*Δ*psd2*Δ in synthetic complete ethanol-glycerol (SCEG) medium with or without 2mM ethanolamine supplementation (Fig 1A). Consistent with previous findings (1, 11, 27), we found that exogenous ethanolamine supplementation restored respiratory growth of *psd1*Δ*psd2*Δ yeast to *psd1*Δ levels but failed to fully restore the respiratory defect associated with *psd1*Δ yeast. Importantly, this basic result was confirmed in *psd1*Δ yeast made in three additional yeast strain backgrounds (Fig 1B). Thus, these findings indicate that the Kennedy pathway cannot fully compensate for the absence of Psd1p function, potentially due to inefficient trafficking of PE from the ER to mitochondrial OM and/or from the OM to the IM.

Validation of constructs that re-direct Psd1p to OM or ER membranes

To interrogate whether the cytosol and/or the IMS is the barrier that prevents extra-mitochondrially produced PE from replacing PE normally made in the IM, we generated chimeric Psd1p constructs that are localized to either the ER or OM to redirect PS and PE metabolism. As depicted in Fig 2A, these two constructs, and the WT IM-localized Psd1p control (referred to as

137 IM-Psd1p to distinguish it from strains expressing endogenous Psd1p), contain a C-terminal
138 3XFLAG tag to track autocatalytic function of these chimeras by immunodetecting the released
139 Psd1p α subunit. To re-direct Psd1p to the mitochondrial OM, the mitochondrial targeting
140 sequence and transmembrane domain of Psd1p were replaced by the equivalent domains of the
141 single-pass OM resident protein, Tom20p. ER-Psd1p, which is directed to the secretory pathway,
142 was generated by replacing the mitochondrial targeting sequence of Psd1p with the NH_2-terminal
143 signal sequence of carboxypeptidase Y as mentioned above (30). The ER-Psd1p construct
144 additionally contains an *N*-glycosylation signal immediately downstream of the CPY leader
145 sequence to track its topology. OM-Psd1p and ER-Psd1p each yielded mature β and α subunits as
146 detected by immunoblot of yeast cell extracts demonstrating that self-processing of Psd1p was not
147 impaired by these modifications to its NH_2-terminus (Fig 2B). All three integrated constructs were
148 similarly expressed relative to each other and over-expressed compared to endogenous Psd1p.
149 Importantly, both OM-Psd1p and ER-Psd1p rescued the ethanolamine auxotrophy of
150 *psd1*Δ*psd2*Δ yeast indicating that these constructs are fully functional and capable of generating
151 levels of PE necessary for cellular growth (Fig 2C).

152 Previously, localization of ER-Psd1p was established by virtue of its enrichment in the
153 40,000 x *g* pellet (P40) after subcellular fractionation by gravity centrifugation and its sensitivity
154 to endoglycosidase H, which revealed a mobility shift following SDS-PAGE post-treatment (30).
155 To confirm the OM localization of OM-Psd1p, its protease accessibility was determined in intact
156 mitochondria, OM-ruptured mitoplasts, and detergent-solubilized mitochondria and compared to
157 IM-Psd1p. Protease treatment of intact mitochondria expressing IM-Psd1p showed protection
158 against degradation of IM-Psd1p and the IM control, Tim54p (Fig 2D). In contrast, similar to the
159 OM control Tom70p, OM-Psd1p was completely degraded in intact mitochondria verifying that it

was successfully re-localized to the OM with the bulk of the enzyme facing the cytosol. As expected given the presence of inter-organelle contact sites, a proportion of ER-Psd1p co-fractionated with crude mitochondria (Fig S1A) and demonstrated protease-sensitivity in intact mitochondria (Fig 2D), a topology that is consistent with its N-glycosylation status (Fig 2E). Thus, a portion of ER-Psd1p is retained in the ER and/or resides in an endosomal compartment that is co-purified with mitochondria.

OM-Psd1p and ER-Psd1p generate levels of PE in mitochondrial membranes that exceed WT

Next, the lipid content of cellular and mitochondrial membranes was assessed in WT, *psd1*Δ, *psd2*Δ, *psd1*Δ*psd2*Δ, IM-Psd1, OM-Psd1 and ER-Psd1 yeast (Fig 3 and Fig S2). The absence of Psd1p resulted in reduced levels of cellular and mitochondrial PE; the combined absence of Psd1p and Psd2p resulted in an additive effect on the steady state abundance of PE (Fig 3D and 3J). In *psd1*Δ and *psd1*Δ*psd2*Δ membranes, the levels of phosphatidylinositol (PI) was increased (Fig 3B and 3H) and cardiolipin (CL) decreased (Fig 3F and 3L), consistent with previous reports (9, 28, 31). Interestingly, a compensatory increase in PS was not detected in these yeast strains, and in fact, the amount of PS was decreased in *psd1*Δ*psd2*Δ mitochondria (Fig 3I). While mitochondrial PE levels were modestly reduced in the absence of Psd2p (Fig 3J), this decrease failed to result in a respiratory growth defect (Fig 1). Combined, these results indicate that Psd2p contributes to the pool of PE associated with mitochondria but is somehow unable to functionally replace PE made by Psd1p.

Interestingly, OM-Psd1 and ER-Psd1 yeast contained significantly higher relative amounts of PE than IM-Psd1 in both cellular and mitochondrial membranes (Fig 3D and 3J). As IM-Psd1p, OM-Psd1p, and ER-Psd1p are similarly over-expressed, this suggests that OM-Psd1p and ER-Psd1p, which are either present in compartments where PS is made (ER-Psd1p) or through which

183 PS must traffic to reach IM-Psd1p (OM-Psd1p), have short-circuited normal mitochondrial PE
184 metabolism. In support of this interpretation, the levels of mitochondrial PS were increased by
185 OM-Psd1p but not ER-Psd1p (Fig 3I), consistent with a mitochondrial trafficking requirement for
186 the former, but not the latter, chimera. The relative abundance of PC was reduced in OM-Psd1 and
187 ER-Psd1, which also failed to restore CL levels to normal. The reduced levels of PC in OM-Psd1
188 and ER-Psd1 is notable as it might have been predicted that an increased production of PE would
189 have resulted in augmented PC synthesis by Pem1p and Pem2p, methyltransferases which reside
190 in the ER and convert PE to PC (32). Overall, the increased levels of PE detected in OM-Psd1 and
191 ER-Psd1 suggests that both chimeras have increased access to substrate compared to IM-Psd1.
192 This conclusion is bolstered both by the fact that overexpressed IM-Psd1p only restored PE to WT
193 levels (Fig 3 D and J), as well as results from a prior study that used a plasmid-based
194 overexpression system (1). Thus, access to substrate is a major regulatory component that
195 determines Psd1p activity.

196 A limitation of the radiolabeling-based phospholipid analysis is that it utilized crude
197 mitochondria generated following physical disruption of intact yeast with glass beads. As such,
198 phospholipid analyses were additionally performed using sucrose gradient purified mitochondria
199 derived from non-radiolabeled yeast cultures. Sucrose purification resulted in mitochondria that
200 were enriched in mitochondrial proteins compared to crude mitochondria (Fig S3A). Subsequent
201 phospholipid analyses of the sucrose purified mitochondria provided a profile that was consistent
202 with results derived using crude mitochondria (Fig 3), with one notable exception: the PE levels
203 were roughly equal in OM-Psd1 and ER-Psd1 sucrose purified mitochondria (Fig S3E). The
204 reduced amounts of mitochondrial PE in ER-Psd1 following sucrose purification likely reflects
205 their increased purity and provides evidence that PE made in the ER can access mitochondrial

206 membranes. Overall, re-routing Psd1p to either the OM or ER results in a robust increase in cellular
207 and mitochondrial PE levels which may or may not reach the mitochondrial IM.

208 *OM-Psd1 and ER-Psd1 phenocopy the respiratory defect of psd1Δ yeast*

209 We initially evaluated oxidative phosphorylation in these strains by determining their
210 growth on synthetic mediums containing dextrose -/+ 2mM ethanolamine, lactate, or
211 ethanol/glycerol -/+ 2mM ethanolamine (Fig 4A). Compared to IM-Psd1p, OM-Psd1p and ER-
212 Psd1p only partially improved growth of *psd1*Δ*psd2*Δ yeast on respiratory carbon sources (lactate
213 and ethanol/glycerol). In fact, they supported respiratory growth that was similar to (ER-Psd1p) or
214 slightly better than (OM-Psd1p) *psd1*Δ yeast, but still significantly reduced compared to the WT
215 strain. Interestingly, respiratory growth was slightly better for *psd1*Δ*psd2*Δ yeast expressing OM-
216 Psd1p *versus* ER-Psd1p. The respiratory phenotype of OM-Psd1 and ER-Psd1 yeast suggests that
217 PE made in either the OM or ER cannot functionally replace PE produced in the IM. Indeed,
218 ethanolamine supplementation did not further improve the respiratory growth of either OM-Psd1
219 or ER-Psd1 yeast (Fig 4A).

220 To directly assess OXPHOS capacity in these strains, oxygen consumption was monitored
221 in isolated mitochondria using an O_2 electrode after the addition of ADP and ascorbate tetramethyl-
222 *p*-phenyldiamine (TMPD) which promotes proton pumping by complex IV (Fig 4B-4E). To
223 determine maximal respiratory capacity, carbonyl cyanide *m*-chlorophenyl hydrazine (CCCP) was
224 added after ADP was depleted and mitochondrial respiration had returned from the ADP-
225 stimulated (State 3) to the resting (State 4) respiratory rate. Mitochondria lacking Psd1p, but not
226 Psd2p, had reduced maximal uncoupled respiratory rate compared to WT mitochondria. Even
227 though *psd2*Δ mitochondria consumed O_2 like WT, the combined absence of Psd1p and Psd2p
228 caused a more severe respiratory defect than was observed when only Psd1p was missing. This

229 indicates that in the absence of Psd1p, PE made by Psd2p has some capacity to compensate for
230 Psd1p and can support limited complex IV activity. Interestingly, the uncoupled respiratory rate
231 for OM-Psd1 and ER-Psd1 was significantly improved compared to *psd1*Δ*psd2*Δ mitochondria
232 but still impaired relative to IM-Psd1 (Fig 4B). The respiratory control ratio (RCR) is an indication
233 of how well respiration is coupled to ATP synthesis and is calculated by dividing the ADP-
234 stimulated respiration rate by the resting respiration rate (State 3/State 4). RCR ratios were
235 significantly decreased in *psd1*Δ and *psd1*Δ*psd2*Δ mitochondria but perplexingly, OM-Psd1 and
236 ER-Psd1 displayed a ratio similar to WT and IM-Psd1 levels (Fig 4C). For *psd1*Δ*psd2*Δ yeast
237 expressing OM-Psd1p and ER-Psd1p, the normal RCR stems from the fact that they improved
238 State 3 O_2 consumption more than State 4. Similar to Psd2p in the context of *psd1*Δ yeast, OM-
239 Psd1p and ER-Psd1p significantly improved *psd1*Δ*psd2*Δ respiratory rates to roughly
240 *psd1*Δ levels, indicating that extra-mitochondrial PE can indeed play an important role in
241 enhancing respiration. Combined, these results suggest that defective complex IV function may
242 contribute to the reduced respiratory growth observed when Psd1p is absent from the IM.

243 *Complex IV function in psd1Δpsd2Δ mitochondria is rescued by ER-Psd1p expression*

244 When grown in dextrose, *psd1*Δ and *psd1*Δ*psd2*Δ yeast lose their mitochondrial genome,
245 visualized by formation of petite colonies, at a high frequency (1, 28, 33). Due to this, we harvested
246 mitochondria from cultures grown in rich lactate to select for growth of respiratory competent
247 cells. As expected, mitochondrial DNA (mtDNA) levels were equivalent between strains in these
248 growth conditions (Fig 5A; ρ^0 yeast, which are devoid of mtDNA, served as a negative control).
249 Next, isolated complex IV activity measurements were recorded by monitoring the rate of
250 oxidation of reduced cytochrome *c* in mitochondria solubilized in 0.5% *n*-Dodecyl-β-D-maltoside
251 (DDM). Complex IV activity was significantly decreased in *psd1*Δ, *psd1*Δ*psd2*Δ, and OM-Psd1

252 mitochondria but surprisingly, ER-Psd1 retained WT function (Fig 5B). To determine if the
253 different complex IV activities associated with OM-Psd1 and ER-Psd1 mitochondria reflected
254 changes in its expression, we analyzed the steady state amounts of both nuclear and mtDNA
255 encoded subunits of complex IV (Fig 5F). While the levels of the mtDNA-encoded subunit, Cox2p,
256 was significantly decreased in *psd1*Δ*psd2*Δ and OM-Psd1 strains, the steady state abundance of
257 the two additional mtDNA-encoded subunits, Cox1p and Cox3p, as well as a constituent encoded
258 in the nucleus, Cox4p, was not significantly changed (Fig S4; while the amount of Cox3p was
259 reduced for *psd1*Δ*psd2*Δ and OM-Psd1, it did not achieve statistical significance). Further, blue
260 native-PAGE analyses indicated that complex IV assembly into respiratory supercomplexes that
261 consist of a complex III dimer affiliated with either one or two complex IV monomers (34), was
262 normal regardless of the absence of *PSD1* or *PSD2*, singly or in combination, as reported by others
263 (28), or whether Psd1p was expressed in the IM, OM, or ER (Fig 5C).

264 *Cytochrome bc_1 complex function is impaired when Psd1p is absent from the IM*

265 The ability of ER-Psd1p, but not OM-Psd1p, to rescue complex IV activity to WT levels
266 was surprising given that neither chimeric construct restored respiratory growth of the *psd1*Δ*psd2*Δ
267 strain to this degree (Fig 4A). Therefore, we postulated that the partial respiratory growth rescue
268 of OM-Psd1 and ER-Psd1 could reflect a defect at the level of complex III. Indeed, complex III
269 activity was reduced in *psd1*Δ and significantly decreased in *psd1*Δ*psd2*Δ mitochondrial extracts
270 (Fig 5D). While ER-Psd1p significantly improved complex IV function over that detected in
271 *psd1*Δ*psd2*Δ mitochondria, neither ER-Psd1p or OM-Psd1p supported complex III activity that
272 resembled WT. The reduced complex III activity in *psd1*Δ, *psd1*Δ*psd2*Δ, and *psd1*Δ*psd2*Δ
273 expressing OM-Psd1p or ER-Psd1p did not reflect alterations in the steady state abundance of its
274 subunits (Fig 5F, Cor2p, Rip1p, Qcr6p, and Qcr7p) or its assembly into supercomplexes (Fig 5E)

although there was proportionately more of the smaller supercomplex (III_2IV > III_2IV_2) detected in *psd1*Δ*psd2*Δ mitochondrial extracts. Furthermore, the steady state levels of the complex III electron acceptor cytochrome *c* were normal (Fig 5F and Fig S4M). Similarly, subunits of the coenzyme Q (CoQ) synthome, a macromolecular complex that catalyzes the synthesis of the complex III electron donor CoQ (35), were equal with the exception of Coq1p which was elevated in *psd1*Δ and *psd1*Δ*psd2*Δ mitochondria (Fig 5F and Fig S5A). Evidence in bacteria suggests that elevation of coenzyme Q biosynthesis may be a mechanism to diminish membrane stress (36). Given that reduced coenzyme Q biosynthesis can be rescued by supplementation of yeast with exogenous CoQ_6 (35), we evaluated if decreased levels of CoQ were implicated in the complex III defect. However, CoQ_6 supplementation failed to rescue respiratory growth of *psd1*Δ or *psd1*Δ*psd2*Δ yeast (Fig S6).

PE made by Kennedy pathway can rescue complex IV but not complex III function

As ER-derived PE restores complex IV, but not complex III, function, we isolated *psd1*Δ*psd2*Δ mitochondria from cultures grown in rich lactate, rich lactate + 2mM choline, and rich lactate +2mM ethanolamine, to evaluate the potential impact of PC and PE generation by the Kennedy pathways on complex IV activity (Fig 6A-B). Similar to ER-Psd1, supplementation of *psd1*Δ*psd2*Δ with ethanolamine, but not choline, restored complex IV (Fig 6A), but not complex III (Fig 6B) function to WT levels. Combined, our results indicate that PE, but not PC, made in the ER by the Kennedy pathway (Fig 6A) or in the endosomal system by either Psd2p or ER-Psd1p (Fig 5B), can significantly rescue the severe complex IV dysfunction that occurs in *psd1*Δ*psd2*Δ yeast. Furthermore, they demonstrate a crucial role for PE made in the IM in supporting the full activity of complex III which is otherwise normally expressed and fully assembled.

DISCUSSION

PE levels have been shown to be altered in models of the neurodegenerative disorders Parkinson's Disease (37) and Alzheimer's Disease (38), and recent evidence has implicated the turnover of mammalian Pisd as an important regulatory mechanism that diminishes the proliferation of breast cancer cells (39). Thus, regulation of the Psd pathway is not only important for mitochondrial function but also organismal health and physiology.

Using an assortment of biochemical assays that measure both the combined and individual activities of the respiratory chain complexes, we sought to clarify the respiratory defect associated with *psd1*Δ yeast and whether or not PE made by the Kennedy pathway could rescue it. Two different groups using the same yeast strain background have reported that supplemental ethanolamine rescues (28) or fails to rescue (11) respiratory function of *psd1*Δ yeast. Given these conflicting results, we first tested the ability of ethanolamine supplementation to improve the respiratory growth phenotype of yeast lacking Psd1p. While we observed that growth of *psd1*Δ*psd2*Δ could be rescued on respiratory medium supplemented with ethanolamine, growth after 3 days was delayed and impaired similarly to *psd1*Δ yeast. Thus, although PE generated through the Kennedy pathway could compensate for the absence of Psd2p, it failed to completely replace Psd1p with respect to respiratory growth. Importantly, the inability of ethanolamine to fully restore *psd1*Δ respiratory growth was verified in three distinct yeast strain backgrounds suggesting that genetic differences are not the source for the disparate results reported previously (1, 11, 27, 28). This notion is further supported by the fact that two groups that each utilized *psd1*Δ derived from the same parental strain came to opposite conclusions regarding the rescuing capacity of PE made by the Kennedy pathway (11, 28). Interestingly, lyso-PE supplementation (PE containing only one acyl chain) can rescue *psd1*Δ respiratory growth but acts via a separate pathway than the Kennedy pathway (27). Further, lyso-PE has also been demonstrated to reverse

321 the mitochondrial defects associated with RNAi silencing of the mammalian *Pisd* in cell culture
322 (10), and can increase the proliferation rate of the MCF7-RAS breast cancer cell line when Pisd
323 levels are depleted (39). Thus, the different ER-resident PE producing pathways appear to differ
324 with respect to their ability to compensate for the absence of the mitochondrial Psd pathway
325 suggesting that pathway-specific mitochondrial import mechanisms for PE may exist.

326 Our oxidative phosphorylation analyses demonstrated that both OM-Psd1 and ER-Psd1
327 phenocopy the respiratory defect of *psd1*Δ mitochondria. This implies that the IMS is the greatest
328 barrier preventing PE import into the inner membrane. Moreover, we have identified a key
329 oxidative phosphorylation component that is uniquely dependent on the presence of Psd1p in the
330 IM: respiratory complex III. Specifically, we demonstrated that while PE synthesized in the ER–
331 by ER-Psd1p, Psd2p, or the Kennedy pathway– can rescue the impaired complex IV activity that
332 occurs in the absence of Psd1p in the IM, it fails to do so for complex III (Fig 6C). Furthermore,
333 this pinpoints defective complex III function as the main culprit responsible for the respiratory
334 growth defect of *psd1*Δ yeast, which cannot be rescued by ethanolamine. Thus, our results strongly
335 indicate that when Psd1p is missing or mis-localized, a minimal threshold of PE is not achieved
336 within the IM that is necessary to promote the full activity of the OXPHOS machinery.

337 What is the basis for the capacity of extra-mitochondrially produced PE to rescue complex
338 IV but not complex III function? As both complex III and complex IV are IM residents, one
339 possibility is that these respiratory complexes require different levels of PE within the inner
340 membrane to function appropriately. If true, this would imply that the relative levels of PE in the
341 IM in the strains analyzed are equivalent between WT, *psd2*Δ, and IM-Psd1, similarly depleted in
342 ER-Psd1 and *psd1*Δ, less than *psd1*Δ in OM-Psd1, and almost completely absent in *psd1*Δ*psd2*Δ.
343 Unfortunately, while it is clear that OM-Psd1 and ER-Psd1 mitochondria contain robust levels of

PE, we have yet to determine its steady state distribution between the outer and inner membranes. Another possible explanation for the different dependence of complex III and IV function on IM-produced PE could reflect the nature of the PE made in the mitochondrion versus elsewhere. Evidence that polyunsaturated 38:4 and 38:5 PE species are enriched in the mitochondrial inner membrane of HeLa cells has been previously reported (40). While both the Kennedy and Psd pathways have the capacity to produce all diacyl-PE species, the Kennedy pathway preferentially synthesizes mono 34:2 or di-unsaturated 36:3 PE and Pisd mainly generates polyunsaturated 38:4 or 38:5 PE (41). However, *S. cerevisiae* is unable to synthesize complex unsaturated fatty acids and the PE acyl chain pattern is the same between whole cells and isolated mitochondria (42, 43). It is interesting to note that, even though the Kennedy and Psd pathways both share a preference for generating both mono- and di-unsaturated PE in yeast, there is a 10% enrichment of 34:2 PE that contains oleic and palmitoleic acid in crude mitochondria versus ER-derived microsomes (42). Another intriguing possibility is that the synthesis of PE by Psd1p in the IM is somehow directly coupled to the incorporation of this lipid into partially or fully assembled complex III. Recently, a subunit of complex IV was found to associate with the MICOS subunit, Mic19, in mammalian cells by EM tomography and immunoprecipitation (44). As the MICOS complex was suggested to work in concert with Ups2p to regulate mitochondrial PS/PE metabolism in yeast (26), potentially, contact sites between the OM and IM could facilitate the transport of ER-derived PE to complex IV more directly than it can to complex III. Finally, perhaps when PE is absent or limiting in the IM, inhibitory molecules are able to bind complex III and impair its activity. Moving forward, it will be important to distinguish between these non-mutually exclusive models.

Another outstanding question raised by our study is exactly how Psd1p or PE made by Psd1p promotes complex III function. Since *psd1*Δ*psd2*Δ yeast contain normal amounts of

367 cytochrome *c* and CoQ_6 supplementation is without effect with respect to respiratory growth, the
368 underlying respiratory defect is presumed to be intrinsic to complex III. Potentially, Psd1p supports
369 complex III function independent of its role in PE production. Alternatively, PE was identified in
370 a crystal structure of the yeast cytochrome bc_1 complex in association with the essential catalytic
371 subunit cytochrome *b* (Cob1p) as well as the Qcr7p subunit. Qcr7p is associated with the matrix
372 facing surface of Cob1p and it is postulated that hydrogen bonding interactions between the
373 headgroup of PE and Glu82 of Qcr7p may help position the complex vertically within the bilayer.
374 As the second PE is found adjacent to the dimer interface of this complex, the acyl chains of PE
375 are thought to interact with both monomers and assist in dimer formation. Additionally, the acyl
376 chains of PE at the dimer interface could potentially promote quinol-quinone exchange at the Q_i
377 and Q_0 sites. More broadly, during quinol-quinone exchange, sidechain movement of Cob1p is
378 thought to be necessary to transfer protons from His202 to ubiquinone, and perhaps depletion of
379 PE hinders this movement and delays proton flux (45). Notably, a recent cryo-EM analysis of
380 respiratory supercomplexes purified from human cells identified PE at the dimer interface of
381 complex III and in close proximity of the mammalian equivalent of Qcr7p (46), suggesting that
382 the important role of PE for complex III function identified here is likely to be evolutionarily
383 conserved.

384 Further, electron-transfer reactions occur within microsecond-to-millisecond time scales
385 and electron-tunneling between complex III monomers is thought to maximize the efficiency of
386 coupled redox reactions between monomers (47). The generation of the free radical semiquinone
387 during the Q cycle performed by complex III is proposed to be diminished by a mechanism that
388 delays quinol oxidation in the Q_o site when electron transfer is pharmacologically impaired (48).
389 If depletion of PE diminishes the efficiency of electron transfer between complex III monomers or

390 between complex III and its substrates, this could result in diminished complex III function as a
391 means to prevent superoxide production. These structural observations will guide future efforts to
392 determine the role(s) of PE as it relates to complex III activity.
393

MATERIALS AND METHODS

TABLE 1 - Strains used in this work		
Strain	**Genotype**	**Source**
Parental		
GA74-1A	*MAT*a, *his3-11,15, leu2, ura3, trp1, ade8 [rho+, mit+]*	Carla Koehler
Deletions		
psd1Δ	*MAT*a, psd1*Δ::HIS3MX6, leu2, ura3, trp1, ade8 [rho+, mit+]*	Ref. 30
psd2Δ	*MAT*a, psd2*Δ::HIS3MX6, leu2, ura3, trp1, ade8 [rho+, mit+]*	Ref. 30
psd1Δpsd2Δ	*MAT*a, psd2*Δ::HIS3MX6, leu2, ura3, psd1Δ::TRP1, ade8 [rho+, mit+]*	Ref. 30
crd1Δ	*MAT*a, *his3-11,15, leu2, ura3, crd1Δ::TRP1, ade8 [rho+, mit+]*	Ref. 52
ρ^0	*MAT*a, *his3-11,15, leu2, ura3, trp1, ade8 [rho-, mit+]*	This study
Integrations		
psd1Δpsd2Δ::Psd1	*MAT*a, *psd2Δ::HIS3MX6, Psd3XFLAG::LEU2, ura3, psd1Δ::TRP1, ade8 [rho+, mit+]*	Ref. 30
psd1Δpsd2Δ::OM–Psd1	*MAT*a, *psd2Δ::HIS3MX6, Tom20-Psd3XFLAG::LEU2, ura3, psd1Δ::TRP1, ade8 [rho+, mit+]*	This study
psd1Δpsd2Δ::ER–Psd1	*MAT*a, *psd2Δ::HIS3MX6, CPY*mPsd3XFLAG::LEU2, ura3, psd1Δ::TRP1, ade8 [rho+, mit+]*	Ref. 30
Parental/Deletion		
W303	*MAT*a, *his3-11, ura3-1,15, trp-1-1, ade2-1, can1-100 [rho+, mit+]*	Cathy Clarke
psd1Δ W303	*MAT*a, psd1*Δ::HIS3MX6, ura3-1,15, trp1-1, ade2-1, can1-100 [rho+, mit+]*	This study
D2730-10B	*MAT*a, *[rho+, mit+]*	Carla Koehler
psd1Δ D273-10B	*MAT*a, psd1*Δ::KANMX6, [rho+, mit+]*	This study
PTY144 (D273-10B derivative)	*MAT*a, *his3::hisg, leu2-3, ura3-52, trp1-delta1, lys2, ade8 [rho+, mit+, LYS2]*	Peter Thorsness
psd1Δ PTY144	*MAT*a, *psd1Δ::HIS3MX6, leu2-3, ura3-52, trp1-delta1, lys2, ade8 [rho+, mit+, LYS2]*	This study

Yeast strains and growth conditions

All yeast strains used in this study are listed in Table 1 and were derived from GA74-1A unless otherwise noted. Deletion strains were generated by PCR-mediated gene replacement of the entire reading frame as previously described (49). Psd1p containing a COOH-terminal 3XFLAG tag subcloned into pRS305 has been described (17, 30). To re-direct Psd1p to the mitochondrial OM, the first 100 amino acids of Psd1p, encompassing its mitochondrial targeting sequence and transmembrane domain, were replaced by the equivalent domains (amino acids 1-34) of the single-pass OM resident protein, Tom20p. ER-Psd1p, which is directed to the secretory pathway, was

generated by replacing the first 57 amino acids of Psd1p, encompassing its mitochondrial targeting signal (MTS), with the N-terminal signal sequence (amino acids 1-23) of carboxypeptidase Y, as previously described (30). Additionally, the ER-Psd1p construct contains an NXS *N*-glycosylation signal immediately downstream of the CPY leader sequence to track its topology. The IM-Psd1, OM-Psd1, and ER-Psd1 constructs, which all contained the C-terminal 3XFLAG tag, were subcloned into the pRS305 plasmid, linearized, and integrated into the *LEU2* locus in the *psd1*Δ*psd2*Δ background. Clones were selected on synthetic dropout medium (0.17% yeast nitrogen base, 0.5% ammonium sulfate, 0.2% dropout mixture synthetic-leu, 2% dextrose) and verified by immunoblot.

Yeast were grown on YPD (1% yeast extract, 2% tryptone, 2%dextose) plates. To assess the function of the assorted re-directed Psd1p constructs, overnight cultures grown in synthetic complete dextrose (SCD; 0.17% yeast nitrogen base, 0.5% ammonium sulfate, 0.2% complete amino acid mixture, 2% dextrose) supplemented with 2mM ethanolamine hydrochloride were spotted on SCD plates in the absence or presence of 2mM ethanolamine hydrochloride, or spotted onto rich lactate (1% yeast extract, 2% tryptone, 0.05% dextrose, 2% lactic acid, 3.4mM $CaCl_2$-$2H_2O$, 8.5mM NaCl, 2.95mM $MgCl_2$-$6H_2O$, 7.35mM KH_2PO_4, 18.7mM NH_4Cl, pH 5.5), or synthetic complete ethanol glycerol (SCEG; 0.17% yeast nitrogen base, 0.5% ammonium sulfate, 0.2% complete amino acid mixture, 1% ethanol, 3% glycerol) or synthetic complete lactate (SC-LAC; 0.17% yeast nitrogen base, 0.5% ammonium sulfate, 0.2% complete amino acid mixture, 0.05% dextrose, 2% lactic acid, 3.4mM $CaCl_2$-$2H_2O$, 8.5mM NaCl, 2.95mM $MgCl_2$-$6H_2O$, 7.35mM KH_2PO_4, 18.7mM NH_4Cl, pH 5.5) in the absence or presence of 2mM ethanolamine hydrochloride to test respiratory growth.

For CoQ_6 supplementation experiments, starter cultures were growth in SCD + 2mM ethanolamine overnight and diluted to 0.025 OD_{600} in 500µL of either SCEG, SCEG + 2mM ethanolamine, SCEG + 2µM CoQ_6, SCEG + 2µM CoQ_6 + 2mM ethanolamine, SCEG + 10µM CoQ_6, or SCEG + 10µM CoQ_6 + 2mM ethanolamine in duplicate in a 48 well plate. OD_{600} measurements were then recorded every 30 minutes for a period of 48 hours at 30°C using a Tecan Infinite 200 Pro instrument.

Mitochondrial Isolation

Isolation of crude mitochondria was performed as previously described (50). Yeast were selected on rich lactate plates and grown on rich lactate media to prevent the loss of mitochondrial DNA. To improve growth on rich lactate, *psd1*Δ*psd2*Δ yeast were grown in the presence of 2mM choline prior to harvesting mitochondria (except where indicated in Fig 6A,B). Purification of mitochondria by sucrose step gradient was performed as previously described (30).

mtDNA quantitation

DNA was extracted as described (51). In brief, yeast cells were grown for 2 days in rich lactate and the collected cell pellets were vortexed at level 10 for 3 minutes with 200µL breaking buffer (2% Triton X-100 (w/v), 1% SDS (v/v), 100mM NaCl, 10mM Tris pH8.0, 1mM EDTA pH 8.0), 0.3g glass beads, and 200µL phenol/chloroform/isoamyl alcohol at room temperature. The solution was neutralized with the addition of 200µL of TE buffer pH 8.0 and phases were separated by centrifugation at 21,000 x *g* for 5 minutes. The aqueous phase was collected and DNA was precipitated by the addition of 100% ethanol and collected in the pellet after centrifugation at 21,000 x *g* for 3 minutes. The pellets were resuspended in 400µL Tris-EDTA (TE) buffer, pH 8.0 and RNA was digested with the addition of 3µL of 10mg/mL RNAse A and incubation at 37°C for 5 minutes before addition of 10 µL of 4M Ammonium acetate and 1mL 100% ethanol. DNA

pellets were recovered by centrifugation 21,000 x *g* for 3 minutes, dried, and resuspended in 30 µL TE buffer pH 8.0. DNA was stored at -80ºC until ready for use, quantitated, and a portion diluted to 10ng/µL to be used as template in the qPCR reaction. The FastStart Universal SYBR Green Master Rox (Roche) was used for qPCR performed according to the manufacturer's instructions. 50ng of genomic DNA was used as a template and the following primers were used at 100nM concentration in a 20µL reaction: COX1 forward (5′-CTACAGATACAGCATTTCCAAGA-3′), COX1 reverse (5′-GTGCCTGAATAGATGATAATGGT-3′), ACT1 forward (5′-GTATGTGTAAAGCCGGTTTTG-3′), ACT1 reverse (5′- CATGATACCTTGGTGTCTTGG -3′). The reactions were performed in technical duplicate with three biological replicates. After completion of thermocycling in a QuantStudio 6 Flex Real-Time PCR System (Thermo Fisher), melting-curve data was collected to verify PCR specificity. The absence of primer dimers and the Ct value difference between the nuclear (ACT1) and mitochondrial (COX1) target were computed as a measure of the level mitochondrial DNA copy number relative to nuclear genome.

Mitochondrial respiration measurements

Mitochondrial oxygen consumption was measured using a Clark-type oxygen electrode in a magnetically stirred, thermostatically controlled 1.5-mL chamber at 25°C (Oxytherm; Hansatech) as previously described (52) with some variations. 100µg of mitochondria were resuspended in 0.25M sucrose, 0.25mg/mL BSA, 20mM KCl, 20mM Tris-Cl, 0.5mM EDTA, 4mM KH_2PO_4, and 3mM $MgCl_2$, pH 7.2. After addition of 1mM ascorbate + 0.3mM TMPD, state 2 rate was monitored for approximately 30 sec. State 3 respiration was initiated by addition of 50µM ADP. After state 4 rate was measured, 10µM CCCP was added to induce uncoupled respiration, and the rate was followed for either 2 minutes or until oxygen level reached zero.

Complex III and IV Activity Measurements

Complex III and IV activities were measured as described (53, 54). To measure complex III activity, 25μg of mitochondria solubilized in 0.5% (w/v) *n*-dodecyl-β-D-maltoside were added to reaction buffer (50mM KP_i, 2mM EDTA, pH 7.4) with 0.008% (w/v) horse heart cytochrome *c* and 1mM KCN. The reaction was started by adding 100μM decylubiquinol, and the reduction of cytochrome *c* followed at 550nM. Complex IV activity was initiated by adding 5μg of solubilized mitochondria to reaction buffer with 0.008% ferrocytochrome *c* and measured by recording cytochrome *c* oxidation at 550nm.

Antibodies

Most antibodies used in this study were generated by our laboratory or in the laboratories of J. Schatz (University of Basel, Basel, Switzerland) or C. Koehler (UCLA) and have been described previously (3, 50, 52, 54-56). Other antibodies used were mouse anti-Sec62p (kind gift of Dr. David Meyers (UCLA)), mouse anti-FLAG (clone M2, Sigma), anti-Dpm1p (113 686, Abcam), rabbit anti-Qcr7p (57), rabbit antisera reactive to Coq1p (58), Coq4p (59), Coq7p (60), or Coq9p (61) and horseradish peroxidase-conjugated (Thermo Fisher Scientific) or IRDye 800CW (LI-COR) secondary antibodies.

Miscellaneous

Preparation of yeast cell extracts, submitochondrial fractionation, phospholipid analysis, 1D BN-PAGE, and immunoblotting were performed as described previously (17, 30). Immunoblots using IR 800 CW secondary antibodies were imaged using an Odyssey CLx Imaging System. Immunoblots and TLC plates were quantitated by Quantity One Software by Bio-Rad Laboratories. Statistical comparisons (ns, $P > 0.05$; 1 symbol $P \leq 0.05$; 2 symbols $P \leq 0.01$; 3 symbols $P \leq 0.001$; 4 symbols $P \leq 0.0001$) were performed by student *t* test or one-way analysis

of variance (ANOVA) with Holm-Sidak pairwise comparison using SigmaPlot 11 software (Systat Software, San Jose, CA); $P \leq 0.05$ were deemed significant. All graphs show the mean $\pm$ S.E.M.

ACKNOWLEDGEMENTS

We would like to thank Drs. Carla Koehler (UCLA), Cathy Clarke (UCLA), Martin Ott (Stockholm University) for antibodies, Drs. Ya-Wen Lu, Ouma Onguka, Seun Ogunbona, and Matthew G. Baile for technical assistance, and Erica Avery for revision of this manuscript. The authors declare no competing financial interests.

REFERENCES

1. Birner R, Burgermeister M, Schneiter R, Daum G. Roles of phosphatidylethanolamine and of its several biosynthetic pathways in Saccharomyces cerevisiae. Mol Biol Cell. 2001;12(4):997-1007. Epub 2001/04/11.
2. Horvath SE, Bottinger L, Vogtle FN, Wiedemann N, Meisinger C, Becker T, et al. Processing and topology of the yeast mitochondrial phosphatidylserine decarboxylase 1. J Biol Chem. 2012;287(44):36744-55. Epub 2012/09/18.
3. Tamura Y, Onguka O, Itoh K, Endo T, Iijima M, Claypool SM, et al. Phosphatidylethanolamine biosynthesis in mitochondria: phosphatidylserine (PS) trafficking is independent of a PS decarboxylase and intermembrane space proteins UPS1P and UPS2P. J Biol Chem. 2012;287(52):43961-71. Epub 2012/11/06.
4. Zborowski J, Dygas A, Wojtczak L. Phosphatidylserine decarboxylase is located on the external side of the inner mitochondrial membrane. FEBS Lett. 1983;157(1):179-82. Epub 1983/06/27.
5. Trotter PJ, Voelker DR. Identification of a non-mitochondrial phosphatidylserine decarboxylase activity (PSD2) in the yeast Saccharomyces cerevisiae. J Biol Chem. 1995;270(11):6062-70. Epub 1995/03/17.
6. Calzada E, Onguka O, Claypool SM. Phosphatidylethanolamine Metabolism in Health and Disease. Int Rev Cell Mol Biol. 2016;321:29-88. Epub 2016/01/27.
7. Steenbergen R, Nanowski TS, Beigneux A, Kulinski A, Young SG, Vance JE. Disruption of the phosphatidylserine decarboxylase gene in mice causes embryonic lethality and mitochondrial defects. J Biol Chem. 2005;280(48):40032-40. Epub 2005/09/30.
8. Fullerton MD, Hakimuddin F, Bakovic M. Developmental and metabolic effects of disruption of the mouse CTP:phosphoethanolamine cytidylyltransferase gene (Pcyt2). Mol Cell Biol. 2007;27(9):3327-36. Epub 2007/02/28.

529 9. Bottinger L, Horvath SE, Kleinschroth T, Hunte C, Daum G, Pfanner N, et al.
530 Phosphatidylethanolamine and cardiolipin differentially affect the stability of mitochondrial
531 respiratory chain supercomplexes. J Mol Biol. 2012;423(5):677-86. Epub 2012/09/14.
532 10. Tasseva G, Bai HD, Davidescu M, Haromy A, Michelakis E, Vance JE.
533 Phosphatidylethanolamine deficiency in Mammalian mitochondria impairs oxidative
534 phosphorylation and alters mitochondrial morphology. J Biol Chem. 2013;288(6):4158-73. Epub
535 2012/12/20.
536 11. Chan EY, McQuibban GA. Phosphatidylserine decarboxylase 1 (Psd1) promotes
537 mitochondrial fusion by regulating the biophysical properties of the mitochondrial membrane and
538 alternative topogenesis of mitochondrial genome maintenance protein 1 (Mgm1). J Biol Chem.
539 2012;287(48):40131-9. Epub 2012/10/10.
540 12. Joshi AS, Thompson MN, Fei N, Huttemann M, Greenberg ML. Cardiolipin and
541 mitochondrial phosphatidylethanolamine have overlapping functions in mitochondrial fusion in
542 Saccharomyces cerevisiae. J Biol Chem. 2012;287(21):17589-97. Epub 2012/03/22.
543 13. Burgermeister M, Birner-Grunberger R, Nebauer R, Daum G. Contribution of different
544 pathways to the supply of phosphatidylethanolamine and phosphatidylcholine to mitochondrial
545 membranes of the yeast Saccharomyces cerevisiae. Biochim Biophys Acta. 2004;1686(1-2):161-
546 8. Epub 2004/11/04.
547 14. Gulshan K, Shahi P, Moye-Rowley WS. Compartment-specific synthesis of
548 phosphatidylethanolamine is required for normal heavy metal resistance. Mol Biol Cell.
549 2010;21(3):443-55. Epub 2009/12/18.
550 15. Di Bartolomeo F, Wagner A, Daum G. Cell biology, physiology and enzymology of
551 phosphatidylserine decarboxylase. Biochim Biophys Acta. 2017;1862(1):25-38. Epub 2016/09/22.
552 16. Choi JY, Duraisingh MT, Marti M, Ben Mamoun C, Voelker DR. From Protease to
553 Decarboxylase: THE MOLECULAR METAMORPHOSIS OF PHOSPHATIDYLSERINE
554 DECARBOXYLASE. J Biol Chem. 2015;290(17):10972-80. Epub 2015/03/01.
555 17. Ogunbona OB, Onguka O, Calzada E, Claypool SM. Multitiered and Cooperative
556 Surveillance of Mitochondrial Phosphatidylserine Decarboxylase 1. Mol Cell Biol. 2017;37(17).
557 Epub 2017/06/14.
558 18. Vance JE. Phospholipid synthesis in a membrane fraction associated with mitochondria. J
559 Biol Chem. 1990;265(13):7248-56. Epub 1990/05/05.
560 19. Voelker DR. Phosphatidylserine functions as the major precursor of
561 phosphatidylethanolamine in cultured BHK-21 cells. Proc Natl Acad Sci U S A. 1984;81(9):2669-
562 73. Epub 1984/05/01.
563 20. Elbaz-Alon Y, Rosenfeld-Gur E, Shinder V, Futerman AH, Geiger T, Schuldiner M. A
564 dynamic interface between vacuoles and mitochondria in yeast. Dev Cell. 2014;30(1):95-102.
565 Epub 2014/07/16.
566 21. Kojima R, Endo T, Tamura Y. A phospholipid transfer function of ER-mitochondria
567 encounter structure revealed in vitro. 2016;6:30777.
568 22. Kornmann B, Currie E, Collins SR, Schuldiner M, Nunnari J, Weissman JS, et al. An ER-
569 mitochondria tethering complex revealed by a synthetic biology screen. Science.
570 2009;325(5939):477-81. Epub 2009/06/27.
571 23. Lahiri S, Chao JT, Tavassoli S, Wong AK, Choudhary V, Young BP, et al. A conserved
572 endoplasmic reticulum membrane protein complex (EMC) facilitates phospholipid transfer from
573 the ER to mitochondria. PLoS Biol. 2014;12(10):e1001969. Epub 2014/10/15.

574 24. Nguyen TT, Lewandowska A, Choi JY, Markgraf DF, Junker M, Bilgin M, et al. Gem1
575 and ERMES do not directly affect phosphatidylserine transport from ER to mitochondria or
576 mitochondrial inheritance. Traffic. 2012;13(6):880-90. Epub 2012/03/14.
577 25. Miyata N, Watanabe Y, Tamura Y, Endo T, Kuge O. Phosphatidylserine transport by
578 Ups2–Mdm35 in respiration-active mitochondria. The Journal of Cell Biology. 2016;214(1):77-
579 88.
580 26. Aaltonen MJ, Friedman JR, Osman C, Salin B, di Rago JP, Nunnari J, et al. MICOS and
581 phospholipid transfer by Ups2-Mdm35 organize membrane lipid synthesis in mitochondria. J Cell
582 Biol. 2016;213(5):525-34. Epub 2016/06/01.
583 27. Riekhof WR, Voelker DR. Uptake and utilization of lyso-phosphatidylethanolamine by
584 Saccharomyces cerevisiae. J Biol Chem. 2006;281(48):36588-96. Epub 2006/10/04.
585 28. Baker CD, Basu Ball W, Pryce EN, Gohil VM. Specific requirements of nonbilayer
586 phospholipids in mitochondrial respiratory chain function and formation. Mol Biol Cell.
587 2016;27(14):2161-71. Epub 2016/05/27.
588 29. Johnson LM, Bankaitis VA, Emr SD. Distinct sequence determinants direct intracellular
589 sorting and modification of a yeast vacuolar protease. Cell. 1987;48(5):875-85. Epub 1987/03/13.
590 30. Onguka O, Calzada E, Ogunbona OB, Claypool SM. Phosphatidylserine decarboxylase 1
591 autocatalysis and function does not require a mitochondrial-specific factor. J Biol Chem.
592 2015;290(20):12744-52. Epub 2015/04/02.
593 31. Storey MK, Clay KL, Kutateladze T, Murphy RC, Overduin M, Voelker DR.
594 Phosphatidylethanolamine has an essential role in Saccharomyces cerevisiae that is independent
595 of its ability to form hexagonal phase structures. J Biol Chem. 2001;276(51):48539-48. Epub
596 2001/10/17.
597 32. Kodaki T, Yamashita S. Yeast phosphatidylethanolamine methylation pathway. Cloning
598 and characterization of two distinct methyltransferase genes. J Biol Chem. 1987;262(32):15428-
599 35. Epub 1987/11/15.
600 33. Trotter PJ, Pedretti J, Voelker DR. Phosphatidylserine decarboxylase from Saccharomyces
601 cerevisiae. Isolation of mutants, cloning of the gene, and creation of a null allele. J Biol Chem.
602 1993;268(28):21416-24. Epub 1993/10/05.
603 34. Schagger H, Pfeiffer K. Supercomplexes in the respiratory chains of yeast and mammalian
604 mitochondria. EMBO J. 2000;19(8):1777-83. Epub 2000/04/25.
605 35. He CH, Xie LX, Allan CM, Tran UC, Clarke CF. Coenzyme Q supplementation or over-
606 expression of the yeast Coq8 putative kinase stabilizes multi-subunit Coq polypeptide complexes
607 in yeast coq null mutants. Biochim Biophys Acta. 2014;1841(4):630-44. Epub 2014/01/11.
608 36. Sévin DC, Sauer U. Ubiquinone accumulation improves osmotic-stress tolerance in
609 Escherichia coli. 2014;10:266.
610 37. Wang S, Zhang S, Liou LC, Ren Q, Zhang Z, Caldwell GA, et al.
611 Phosphatidylethanolamine deficiency disrupts alpha-synuclein homeostasis in yeast and worm
612 models of Parkinson disease. Proc Natl Acad Sci U S A. 2014;111(38):E3976-85. Epub
613 2014/09/10.
614 38. Nesic I, Guix FX, Vennekens K, Michaki V, Van Veldhoven PP, Feiguin F, et al.
615 Alterations in phosphatidylethanolamine levels affect the generation of Abeta. Aging Cell.
616 2012;11(1):63-72. Epub 2011/10/26.
617 39. Keckesova Z, Donaher JL, De Cock J, Freinkman E, Lingrell S, Bachovchin DA, et al.
618 LACTB is a tumour suppressor that modulates lipid metabolism and cell state. Nature.
619 2017;543(7647):681-6. Epub 2017/03/23.

620 40. Kainu V, Hermansson M, Hanninen S, Hokynar K, Somerharju P. Import of
621 phosphatidylserine to and export of phosphatidylethanolamine molecular species from
622 mitochondria. Biochim Biophys Acta. 2013;1831(2):429-37. Epub 2012/11/20.
623 41. Bleijerveld OB, Brouwers JF, Vaandrager AB, Helms JB, Houweling M. The CDP-
624 ethanolamine pathway and phosphatidylserine decarboxylation generate different
625 phosphatidylethanolamine molecular species. J Biol Chem. 2007;282(39):28362-72. Epub
626 2007/08/04.
627 42. Burgermeister M, Birner-Grunberger R, Heyn M, Daum G. Contribution of different
628 biosynthetic pathways to species selectivity of aminoglycerophospholipids assembled into
629 mitochondrial membranes of the yeast Saccharomyces cerevisiae. Biochim Biophys Acta.
630 2004;1686(1-2):148-60. Epub 2004/11/04.
631 43. Schneiter R, Brugger B, Sandhoff R, Zellnig G, Leber A, Lampl M, et al. Electrospray
632 ionization tandem mass spectrometry (ESI-MS/MS) analysis of the lipid molecular species
633 composition of yeast subcellular membranes reveals acyl chain-based sorting/remodeling of
634 distinct molecular species en route to the plasma membrane. J Cell Biol. 1999;146(4):741-54.
635 Epub 1999/08/25.
636 44. Sastri M, Darshi M, Mackey M, Ramachandra R, Ju S, Phan S, et al. Sub-mitochondrial
637 localization of the genetic-tagged mitochondrial intermembrane space-bridging components
638 Mic19, Mic60 and Sam50. J Cell Sci. 2017;130(19):3248-60. Epub 2017/08/16.
639 45. Hunte C, Koepke J, Lange C, Rossmanith T, Michel H. Structure at 2.3 A resolution of the
640 cytochrome bc(1) complex from the yeast Saccharomyces cerevisiae co-crystallized with an
641 antibody Fv fragment. Structure. 2000;8(6):669-84. Epub 2000/06/30.
642 46. Guo R, Zong S, Wu M, Gu J, Yang M. Architecture of Human Mitochondrial Respiratory
643 Megacomplex I2III2IV2. Cell. 2017;170(6):1247-57 e12. Epub 2017/08/29.
644 47. Swierczek M, Cieluch E, Sarewicz M, Borek A, Moser CC, Dutton PL, et al. An electronic
645 bus bar lies in the core of cytochrome bc1. Science. 2010;329(5990):451-4. Epub 2010/07/24.
646 48. Quinlan CL, Gerencser AA, Treberg JR, Brand MD. The mechanism of superoxide
647 production by the antimycin-inhibited mitochondrial Q-cycle. J Biol Chem. 2011;286(36):31361-
648 72. Epub 2011/06/29.
649 49. Baile MG, Sathappa M, Lu YW, Pryce E, Whited K, McCaffery JM, et al. Unremodeled
650 and remodeled cardiolipin are functionally indistinguishable in yeast. J Biol Chem.
651 2014;289(3):1768-78. Epub 2013/11/29.
652 50. Claypool SM, McCaffery JM, Koehler CM. Mitochondrial mislocalization and altered
653 assembly of a cluster of Barth syndrome mutant tafazzins. The Journal of cell biology.
654 2006;174(3):379-90. PMCID: PMC2064234. Epub 2006/08/02.
655 51. Hoffman CS. Preparation of yeast DNA. Curr Protoc Mol Biol. 2001;Chapter 13:Unit13.1.
656 52. Claypool SM, Oktay Y, Boontheung P, Loo JA, Koehler CM. Cardiolipin defines the
657 interactome of the major ADP/ATP carrier protein of the mitochondrial inner membrane. J Cell
658 Biol. 2008;182(5):937-50. Epub 2008/09/10.
659 53. Tzagoloff A, Akai A, Needleman RB. Assembly of the mitochondrial membrane system:
660 isolation of nuclear and cytoplasmic mutants of Saccharomyces cerevisiae with specific defects in
661 mitochondrial functions. J Bacteriol. 1975;122(3):826-31. Epub 1975/06/01.
662 54. Baile MG, Whited K, Claypool SM. Deacylation on the matrix side of the mitochondrial
663 inner membrane regulates cardiolipin remodeling. Mol Biol Cell. 2013;24(12):2008-20. Epub
664 2013/05/03.

665 55. Whited K, Baile MG, Currier P, Claypool SM. Seven functional classes of Barth syndrome
666 mutation. Hum Mol Genet. 2013;22(3):483-92. Epub 2012/10/27.
667 56. Riezman H, Hase T, van Loon AP, Grivell LA, Suda K, Schatz G. Import of proteins into
668 mitochondria: a 70 kilodalton outer membrane protein with a large carboxy-terminal deletion is
669 still transported to the outer membrane. EMBO J. 1983;2(12):2161-8. Epub 1983/01/01.
670 57. Hildenbeutel M, Hegg EL, Stephan K, Gruschke S, Meunier B, Ott M. Assembly factors
671 monitor sequential hemylation of cytochrome b to regulate mitochondrial translation.
672 The Journal of Cell Biology. 2014;205(4):511-24.
673 58. Gin P, Clarke CF. Genetic Evidence for a Multi-subunit Complex in Coenzyme Q
674 Biosynthesis in Yeast and the Role of the Coq1 Hexaprenyl Diphosphate Synthase. Journal of
675 Biological Chemistry. 2005;280(4):2676-81.
676 59. Belogrudov GI, Lee PT, Jonassen T, Hsu AY, Gin P, Clarke CF. Yeast COQ4 Encodes a
677 Mitochondrial Protein Required for Coenzyme Q Synthesis. Archives of Biochemistry and
678 Biophysics. 2001;392(1):48-58.
679 60. Tran UC, Marbois B, Gin P, Gulmezian M, Jonassen T, Clarke CF. Complementation of
680 Saccharomyces cerevisiae coq7 Mutants by Mitochondrial Targeting of the Escherichia coli UbiF
681 Polypeptide: TWO FUNCTIONS OF YEAST COQ7 POLYPEPTIDE IN COENZYME Q
682 BIOSYNTHESIS. Journal of Biological Chemistry. 2006;281(24):16401-9.
683 61. Hsieh EJ, Dinoso JB, Clarke CF. A tRNATRP gene mediates the suppression of cbs2-223
684 previously attributed to ABC1/COQ8. Biochemical and Biophysical Research Communications.
685 2004;317(2):648-53.
686
687

688

Main Figure Captions

Fig 1. Ethanolamine supplementation fails to rescue the growth defect of *psd1*Δ on respiratory medium in 4 separate yeast strains. (A,B) The indicated strains were pre-cultured at 30°C in YPD and spotted onto synthetic complete dextrose (SCD) or ethanol glycerol (SCEG) medium +/- 2mM ethanolamine (+E) and incubated at 30°C for 3 days.

Fig 2. OM-Psd1p and ER-Psd1p constructs are functional and localize to the OM and ER, respectfully. (A) Schematic of the construct design for IM-Psd1p, OM-Psd1p, and ER-Psd1p targeted for integration in *psd1Δpsd2Δ*. All three constructs contain a 3XFLAG tag at the C-terminus (yellow). The Tom20 residues (1-100) that replace the mitochondrial targeting sequence (MT) and transmembrane (TM) domain of IM-Psd1p (green) are shown for OM-Psd1p (blue), and the carboxypeptidase Y signal sequence (residues 1-37) as well as an NXS motif are indicated for ER-Psd1p (purple). (B) The β and α subunits of Psd1p were detected in yeast whole cell extracts of the indicated strains by immunoblot. Tom70p serves as a loading control. (C) The indicated strains were spotted onto synthetic complete dextrose (SCD) medium +/- 2mM ethanolamine (+E) and incubated at 30°C for 4 days. (D) Protease protection assay in intact mitochondria (Mito), osmotically ruptured mitochondria (MP), or deoxycholate-solubilized mitochondria (Det.). Following incubation -/+ 100μg proteinase K (Prot. K) for 30 minutes, samples were collected, resolved by SDS-PAGE and immunoblotted for Psd1p (β and α subunits), and the mitochondrial compartment-specific markers Tom70p (OM), Tim54p (IM), and Abf2p (matrix). (E) Illustration indicating the topology of (1) IM-Psd1p, (2) OM-Psd1p, and (3) ER-Psd1p.

Fig 3. OM-Psd1 and ER-Psd1 contain robust levels of PE in both cellular and mitochondrial membranes. (A-F) Cellular and (G-L) mitochondrial phospholipids from the indicated strains

were labeled overnight with $^{32}P_i$ and separated by TLC. All graphs show the mean ± S.E.M. for n=6 biological replicates. Significant differences compared to WT were calculated by one-way ANOVA. (M) Key for symbols used for statistical analysis interpretation by one-way ANOVA when comparing samples *versus* WT (*), *psd1*Δ*psd2*Δ (#), or IM-Psd1 ($).

Fig 4. OM-Psd1 and ER-Psd1 OXPHOS function phenocopies *psd1*Δ. (A) The indicated strains were spotted and incubated at 30°C for 2 days on SCD +/- 2mM ethanolamine (+E) and for 5 days on rich lactate, SC lactate, SCEG and +/- 2mM ethanolamine (+E). (B-E) O_2 consumption measurements from mitochondria isolated from yeast grown in rich lactate using ascorbate-TMPD as a substrate. (B) The maximal respiratory rate was recorded after the addition of CCCP, (D) state 3 respiration was assessed after addition of ADP, and (E) state 4 respiration was recorded following ADP depletion. (C) The respiratory control ratio (RCR) is calculated by dividing state 3 by state 4 respiratory rates. Analysis *versus* WT (*), *psd1*Δ*psd2*Δ (#), or IM-Psd1 ($) was performed by one-way ANOVA ± S.E.M. for n=4.

Fig 5. Complex III and IV activities are impaired when Psd1p is absent in the IM. (A) mtDNA was isolated from the indicated strains, normalized, and quantified by qPCR. Analysis was performed by one-way ANOVA ± S.E.M. for n=3. (B) Spectrophotometric assay following the oxidation of cytochrome *c* at 550nM in isolated mitochondria solubilized in 0.5% DDM. Analysis *versus* WT (*), *psd1*Δ*psd2*Δ (#), or IM-Psd1 ($) was performed by one-way ANOVA ± S.E.M. for n=6. P values for decreases that didn't achieve significance are reported in red and were analyzed by student *t*-test *versus* WT. (C) Blue native-PAGE analysis of mitochondrial extracts solubilized in 1.5% digitonin. Complex IV assembly was monitored by immunoblot against the

nuclear-encoded subunit Cox4p. (D) Spectrophotometric assay following the reduction of cytochrome *c* at 550nM in isolated mitochondria solubilized in 0.5% DDM. Analysis *versus* WT (*), *psd1*Δ*psd2*Δ (#), or IM-Psd1 ($) was performed by one-way ANOVA ± S.E.M for n=6. P values for decreases that didn't achieve significance are reported in red and were analyzed by student *t*-test *versus* WT. (E) Blue native-PAGE analysis of mitochondrial extracts solubilized in 1.5% digitonin. Complex III assembly was monitored by immunoblot against the nuclear-encoded subunit Rip1p. (F) Mitochondria from the indicated strains were immunoblotted for subunits of complex III (CIII), complex IV (CIV), complex V (CV), and the Coq synthome, cytochrome *c*, and markers of each mitochondrial compartment.

Fig 6. PE generated outside the IM can rescue the activity of complex IV but not complex III. Spectrophotometric assay following the (A) oxidation and (B) reduction of cytochrome *c* at 550nM in isolated mitochondria solubilized in 0.5% DDM. Analysis *versus* WT (*), *psd1*Δ*psd2*Δ (#), or IM-Psd1 ($) was performed by one-way ANOVA ± S.E.M. for n=6. P values for decreases that didn't achieve significance are reported in red and were analyzed by student *t*-test. (C) Schematic diagram of changes in complex III and complex IV activities that occur when Psd1p is absent in the IM or re-routed to OM or ER membranes. PE^1 indicates PE synthesized within the IM by Psd1p; PE^2 symbolizes PE generated outside the IM by either Psd2p, the Kennedy pathway, OM-Psd1p, or ER-Psd1p; IL indicates inhibitory lipids or molecules that may inhibit complex III activity when Psd1p is absent.

Supplemental Figures - Captions

Fig S1. ER-Psd1p co-fractionates with ER/endosomal compartment. (A) Following growth in rich lactate medium to late log phase, fractions were collected from the indicated yeast strains by differential gravity centrifugation. Equal protein amounts from each collected fraction were resolved by SDS-PAGE and immunoblotted for Psd1p (β and α subunits) and markers for each compartment (Kgd1p for mitochondria/P13, Sec62p for the ER/P40, and Hsp70 for the cytosol/S40.

Fig S2. TLC images of $^{32}P_i$-labeled lipids. Representative TLC plates from (A) Cellular and (B) mitochondrial lipid extractions. The migration of different phospholipid classes is indicated.

Fig S3. Phospholipid analysis of sucrose gradient purified mitochondria indicates equivalent levels of PE in OM-Psd1 and ER-Psd1 mitochondria. (A) After crude isolation of mitochondria by gravity centrifugation, samples were overlaid on a two-step sucrose gradient containing 32% and 60% sucrose in EM buffer and subjected to ultracentrifugation at 134,000 x *g* for 1 hour at 4°C. Purification of mitochondria was monitored by using the mitochondrial marker Tom70p and the endosomal marker Dpm1p. (B) Total phospholipid content/mitochondrial protein (mean ± S.E.M., n =4) in sucrose purified mitochondria.(C-F) Quantitation of phospholipid levels after separation by TLC and visualization by molybdenum blue staining. Analysis *versus* WT (*), *psd1*Δ*psd2*Δ (#), or IM-Psd1 ($) was performed by one-way ANOVA ± S.E.M. for n=4. (G) Representative TLC plate of phospholipid extraction from sucrose purified mitochondria followed by visualization using molybdenum blue reagent.

Fig S4. Quantitation of respiratory complex subunits. Densitometry analysis of steady state protein amounts in isolated mitochondria (30 μg) from the indicated strains (representative immunoblots shown in Fig 5F). Analysis *versus* WT (*), *psd1*Δ*psd2*Δ (#), or IM-Psd1 ($) was performed by one-way ANOVA ± S.E.M. for n=4.

Fig S5. Quantitation of CoQ synthome subunits and additional mitochondrial proteins. Densitometry analysis of steady state protein amounts in isolated mitochondria (30 μg) from the indicated strains (representative immunoblots shown in Fig 5F). Analysis *versus* WT (*) or *psd1*Δ*psd2*Δ (#) was performed by one-way ANOVA ± S.E.M. for n=4.

Fig S6. CoQ_6 supplementation does not rescue the *psd1Δ* and *psd1Δ psd2Δ* growth defects on respiratory medium. OD_{600} measurements were recorded every 30 minutes for a period of 48 hours at 30°C for yeast grown in (A) SCEG, (B) SCEG + 2mM ethanolamine (eth), (C) SCEG + 2μM CoQ_6, (D) SCEG + 2μM CoQ_6 + 2mM ethanolamine, (E) SCEG + 10μM CoQ_6, and (F) SCEG + 10μM CoQ_6 + 2mM ethanolamine. ± S.E.M. for n=2.

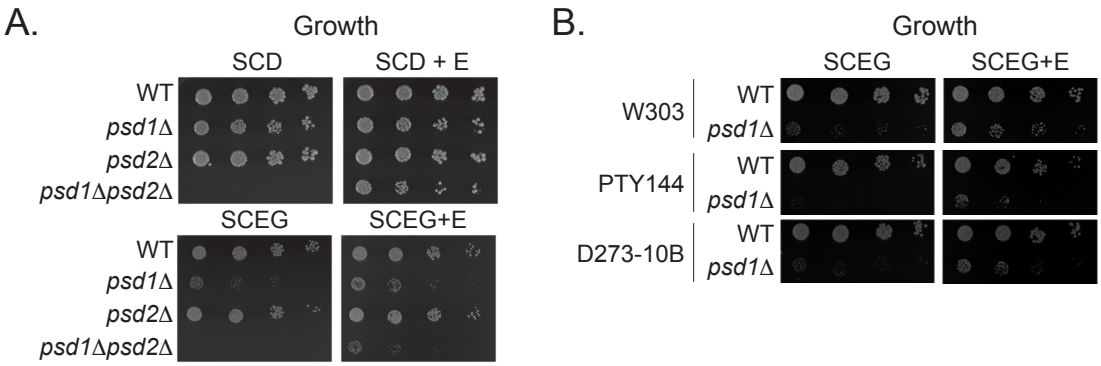

Fig 1. Ethanolamine supplementation fails to rescue the growth defect of *psd1*Δ on respiratory medium in 4 separate yeast strains. (A,B) The indicated strains were pre-cultured at 30°C in YPD and spotted onto synthetic complete dextrose (SCD) or ethanol glycerol (SCEG) medium +/- 2mM ethanolamine (+E) and incubated at 30°C for 3 days.

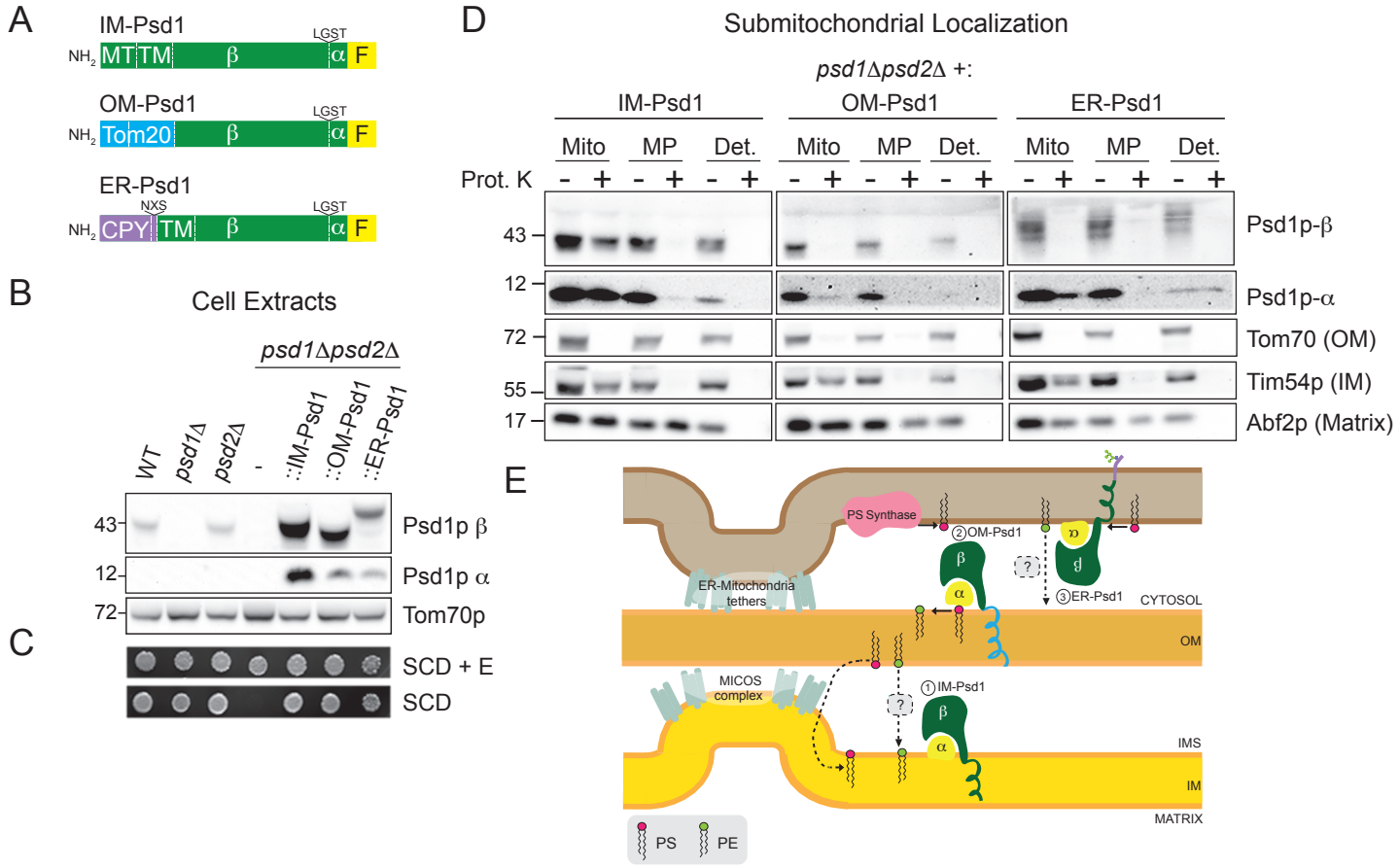

Fig 2. OM-Psd1p and ER-Psd1p constructs are functional and localize to the OM and ER, respectfully. (A) Schematic of the construct design for IM-Psd1p, OM-Psd1p, and ER-Psd1p targeted for integration in *psd1Δpsd2Δ*. All three constructs contain a 3XFLAG tag at the C-terminus (yellow). The Tom20 residues (1-100) that replace the mitochondrial targeting sequence (MT) and transmembrane (TM) domain of IM-Psd1p (green) are shown for OM-Psd1p (blue), and the carboxypeptidase Y signal sequence (residues 1-37) as well as an NXS motif are indicated for ER-Psd1p (purple). (B) The β and α subunits of Psd1p were detected in yeast whole cell extracts of the indicated strains by immunoblot. Tom70p serves as a loading control. (C) The indicated strains were spotted onto synthetic complete dextrose (SCD) medium +/- 2mM ethanolamine (+E) and incubated at 30°C for 4 days. (D) Protease protection assay in intact mitochondria (Mito), osmotically ruptured mitochondria (MP), or deoxycholate-solubilized mitochondria (Det.). Following incubation -/+ 100μg proteinase K (Prot. K) for 30 minutes, samples were collected, resolved by SDS-PAGE and immunoblotted for Psd1p (β and α subunits), and the mitochondrial compartment-specific markers Tom70p (OM), Tim54p (IM), and Abf2p (matrix). (E) Illustration indicating the topology of (1) IM-Psd1p, (2) OM-Psd1p, and (3) ER-Psd1p.

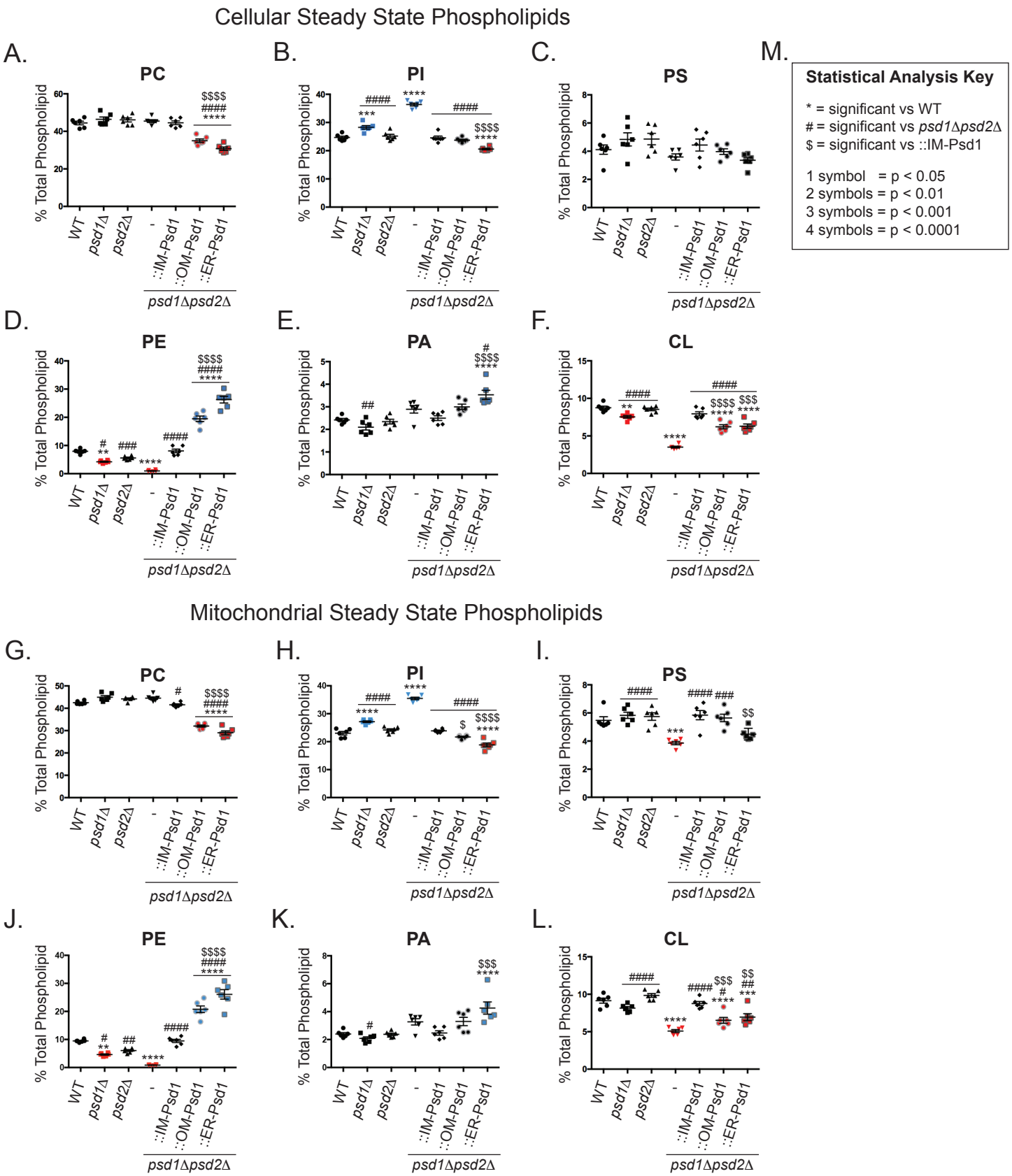

Fig 3. OM-Psd1 and ER-Psd1 contain robust levels of PE in both cellular and mitochondrial membranes. (A-F) Cellular and (G-L) mitochondrial phospholipids from the indicated strains were labeled overnight with 32^{Pi} and separated by TLC. All graphs show the mean ± S.E.M. for n=6 biological replicates. Significant differences compared to WT were calculated by one-way ANOVA. (M) Key for symbols used for statistical analysis interpretation by one-way ANOVA when comparing samples *versus* WT (*), *psd1Δpsd2Δ* (#), or IM-Psd1 ($).

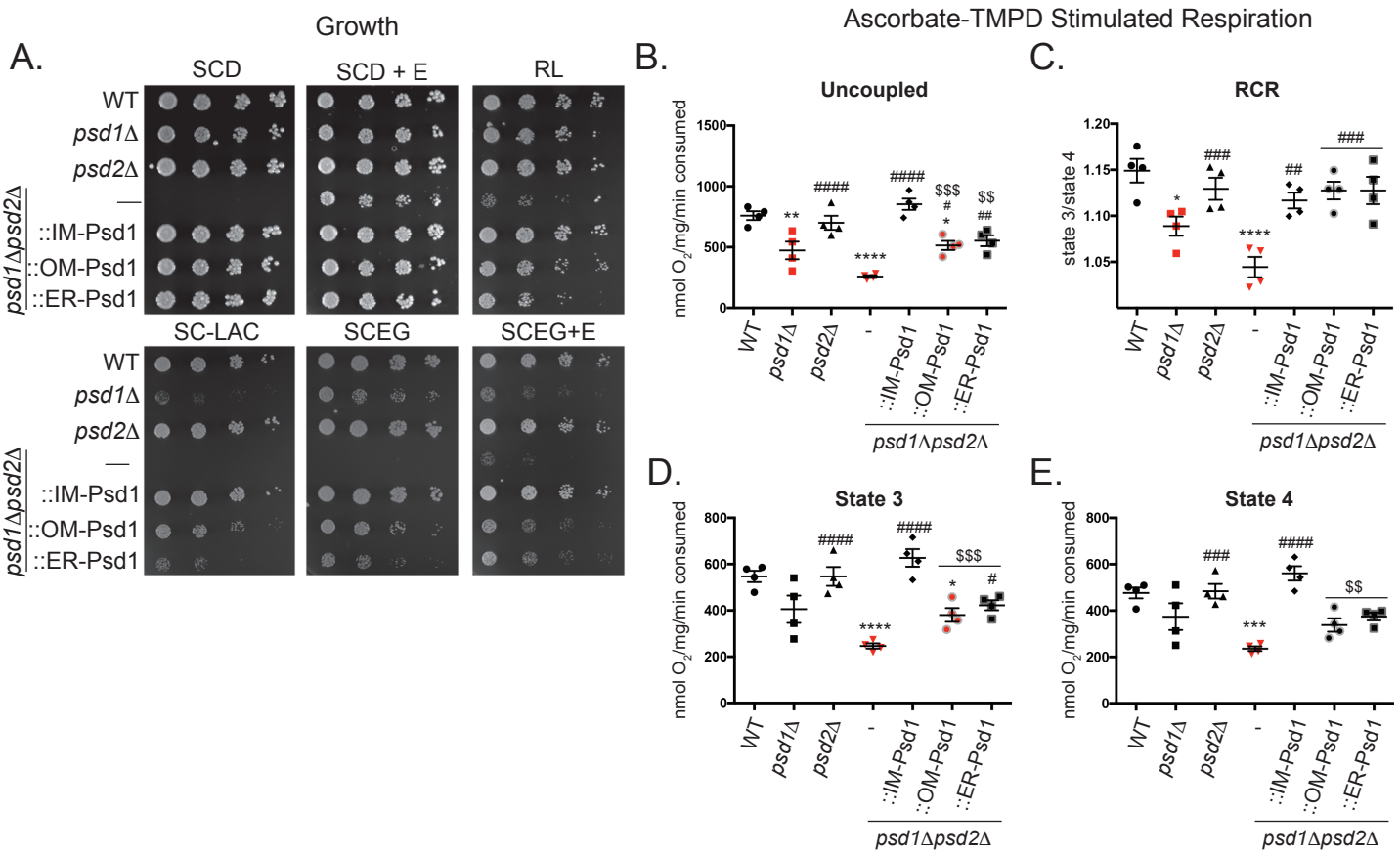

Fig 4. OM-Psd1 and ER-Psd1 OXPHOS function phenocopies *psd1*Δ. (A) The indicated strains were spotted and incubated at 30°C for 2 days on SCD +/- 2mM ethanolamine (+E) and for 5 days on rich lactate, SC lactate, SCEG and +/- 2mM ethanolamine (+E). (B-E) O_2 consumption measurements from mitochondria isolated from yeast grown in rich lactate using ascorbate-TMPD as a substrate. (B) The maximal respiratory rate was recorded after the addition of CCCP, (D) state 3 respiration was assessed after addition of ADP, and (E) state 4 respiration was recorded following ADP depletion. (C) The respiratory control ratio (RCR) is calculated by dividing state 3 by state 4 respiratory rates. Analysis *versus* WT (*), *psd1*Δ*psd2*Δ (#), or IM-Psd1 ($) was performed by one-way ANOVA ± S.E.M. for n=4.

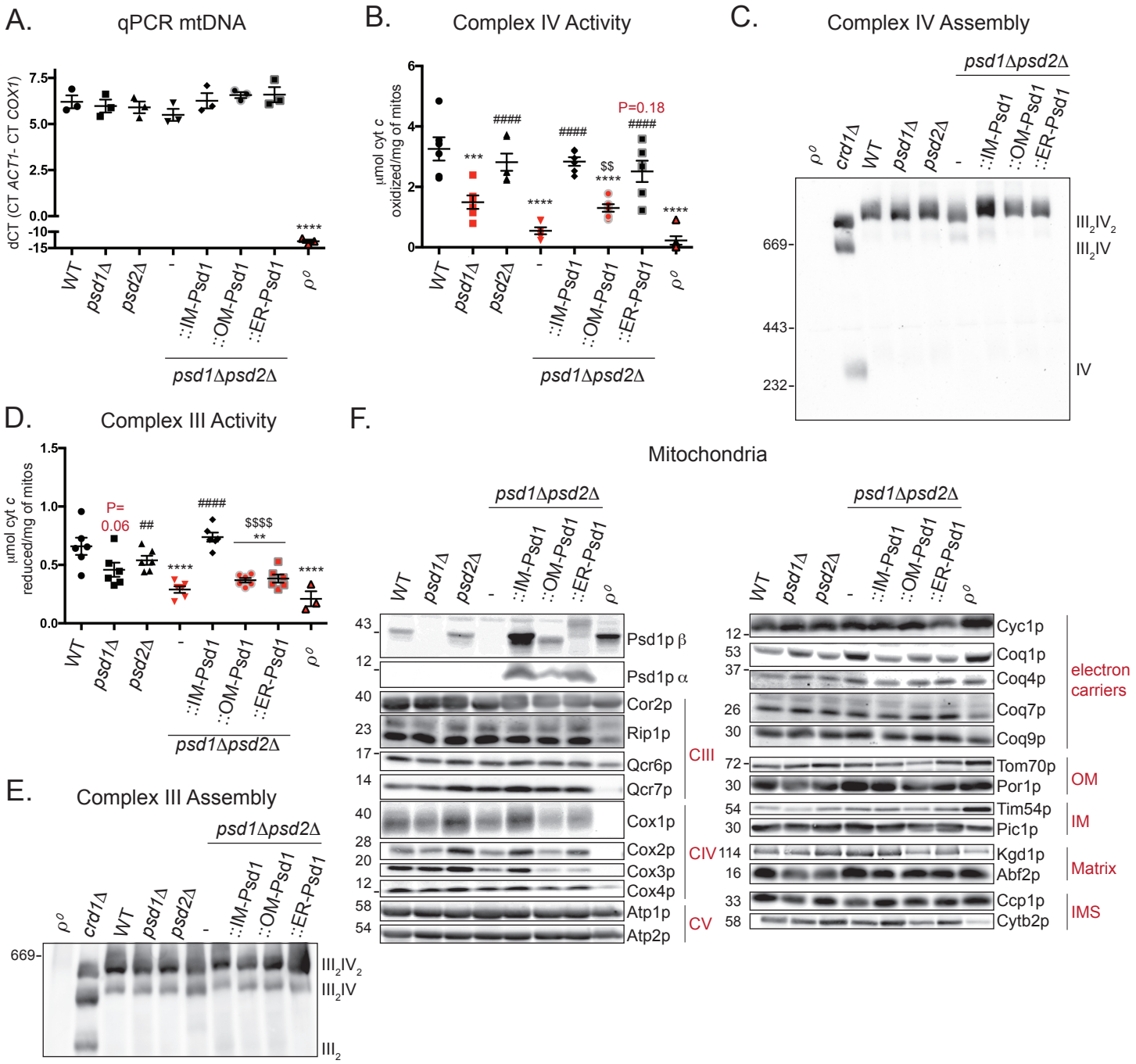

Fig 5. Complex III and IV activities are impaired when Psd1p is absent in the IM. (A) mtDNA was isolated from the indicated strains, normalized, and quantified by qPCR. Analysis was performed by one-way ANOVA ± S.E.M. for n=3. (B) Spectrophotometric assay following the oxidation of cytochrome *c* at 550nM in isolated mitochondria solubilized in 0.5% DDM. Analysis *versus* WT (*), *psd1Δpsd2Δ* (#), or IM-Psd1 ($) was performed by one-way ANOVA ± S.E.M. for n=6. P values for decreases that didn't achieve significance are reported in red and were analyzed by student *t*-test versus WT. (C) Blue native-PAGE analysis of mitochondrial extracts solubilized in 1.5% digitonin. Complex IV assembly was monitored by immunoblot against the nuclear-encoded subunit Cox4p. (D) Spectrophotometric assay following the reduction of cytochrome *c* at 550nM in isolated mitochondria solubilized in 0.5% DDM. Analysis *versus* WT (*), *psd1Δpsd2Δ* (#), or IM-Psd1 ($) was performed by one-way ANOVA ± S.E.M. for n=6. P values for decreases that didn't achieve significance are reported in red and were analyzed by student *t*-test versus WT. (E) Blue native-PAGE analysis of mitochondrial extracts solubilized in 1.5% digitonin. Complex III assembly was monitored by immunoblot against the nuclear-encoded subunit Rip1p. (F) Mitochondria from the indicated strains were immunoblotted for subunits of complex III (CIII), complex IV (CIV), complex V (CV), and the Coq synthome, cytochrome *c*, and markers of each mitochondrial compartment.

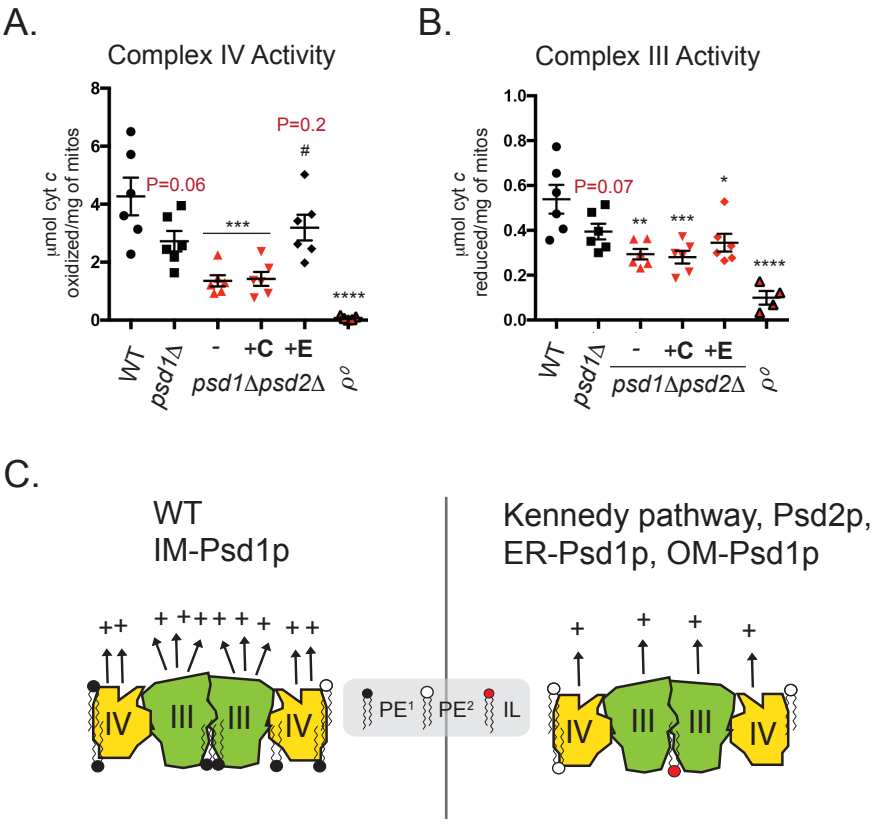

Fig 6. PE generated outside the IM can rescue the activity of complex IV but not complex III. Spectrophotometric assay following the (A) oxidation and (B) reduction of cytochrome *c* at 550nM in isolated mitochondria solubilized in 0.5% DDM. Analysis *versus* WT (*), *psd1Δpsd2Δ* (#), or IM-Psd1 ($) was performed by one-way ANOVA ± S.E.M. for n=6. P values for decreases that didn't achieve significance are reported in red and were analyzed by student *t*-test. (C) Schematic diagram of changes in complex III and complex IV activities that occur when Psd1p is absent in the IM or re-routed to OM or ER membranes. PE^1 indicates PE synthesized within the IM by Psd1p; PE^2 symbolizes PE generated outside the IM by either Psd2p, the Kennedy pathway, OM-Psd1p, or ER-Psd1p; IL indicates inhibitory lipids or molecules that may inhibit complex III activity when Psd1p is absent.

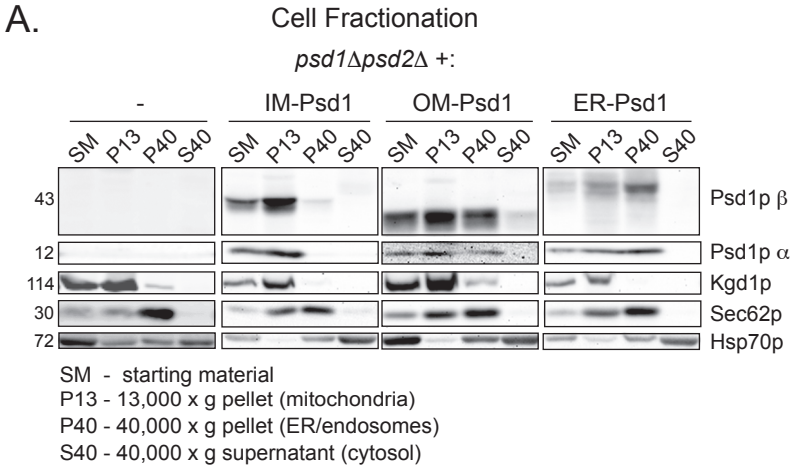

Fig S1. ER-Psd1p co-fractionates with ER/endosomal compartment. (A) Following growth in rich lactate medium to late log phase, fractions were collected from the indicated yeast strains by differential gravity centrifugation. Equal protein amounts from each collected fraction were resolved by SDS-PAGE and immunoblotted for Psd1p (β and α subunits) and markers for each compartment (Kgd1p for mitochondria/P13, Sec62p for the ER/P40, and Hsp70 for the cytosol/S40.

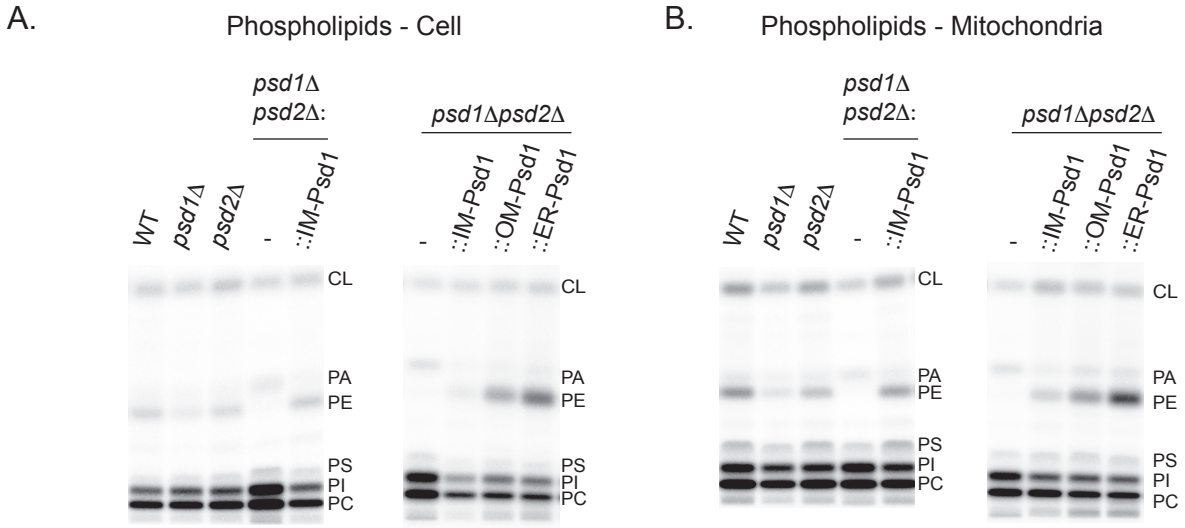

Fig S2. TLC images of 32^{Pi}-labeled lipids. Representative TLC plates from (A) Cellular and (B) mitochondrial lipid extractions. The migration of different phospholipid classes is indicated.

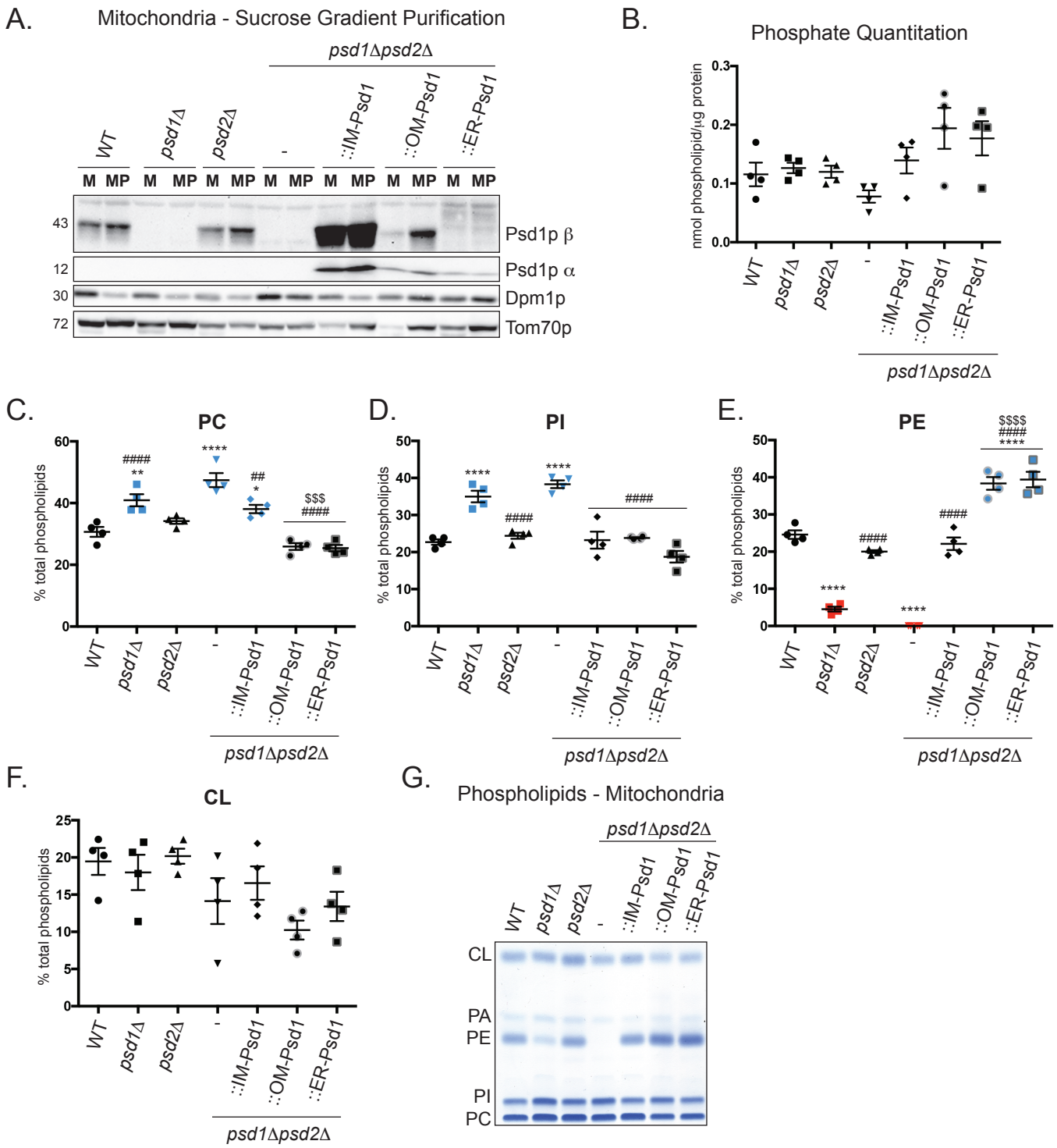

Fig S3. Phospholipid analysis of sucrose gradient purified mitochondria indicates equivalent levels of PE in OM-Psd1 and ER-Psd1 mitochondria. (A) After crude isolation of mitochondria by gravity centrifugation, samples were overlaid on a two-step sucrose gradient containing 32% and 60% sucrose in EM buffer and subjected to ultracentrifugation at 134,000 x g for 1 hour at 4°C. Purification of mitochondria was monitored by using the mitochondrial marker Tom70p and the endosomal marker Dpm1p. (B) Total phospholipid content/mitochondrial protein (mean ± S.E.M., n=4) in sucrose purified mitochondria.(C-F) Quantitation of phospholipid levels after separation by TLC and visualization by molybdenum blue staining. Analysis *versus* WT (*), *psd1Δpsd2Δ* (#), or IM-Psd1 ($) was performed by one-way ANOVA ± S.E.M. for n=4. (G) Representative TLC plate of phospholipid extraction from sucrose purified mitochondria followed by visualization using molybdenum blue reagent.

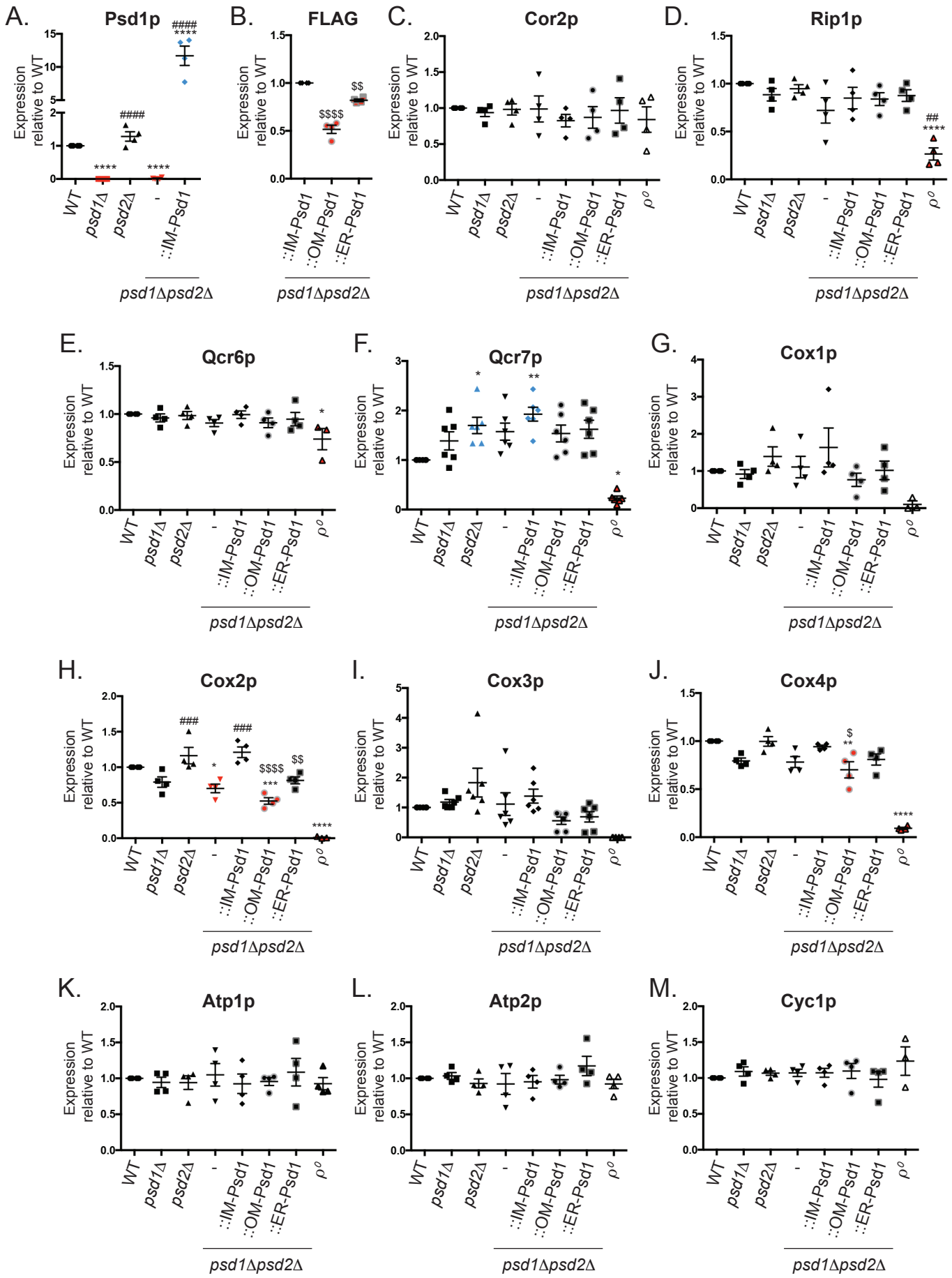

Fig S4. Quantitation of respiratory complex subunits. Densitometry analysis of steady state protein amounts in isolated mitochondria (30 μg) from the indicated strains (representative immunoblots shown in Figure 5F). Analysis *versus* WT (*), *psd1Δpsd2Δ* (#), or IM-Psd1 ($) was performed by one-way ANOVA ± S.E.M. for n=4.

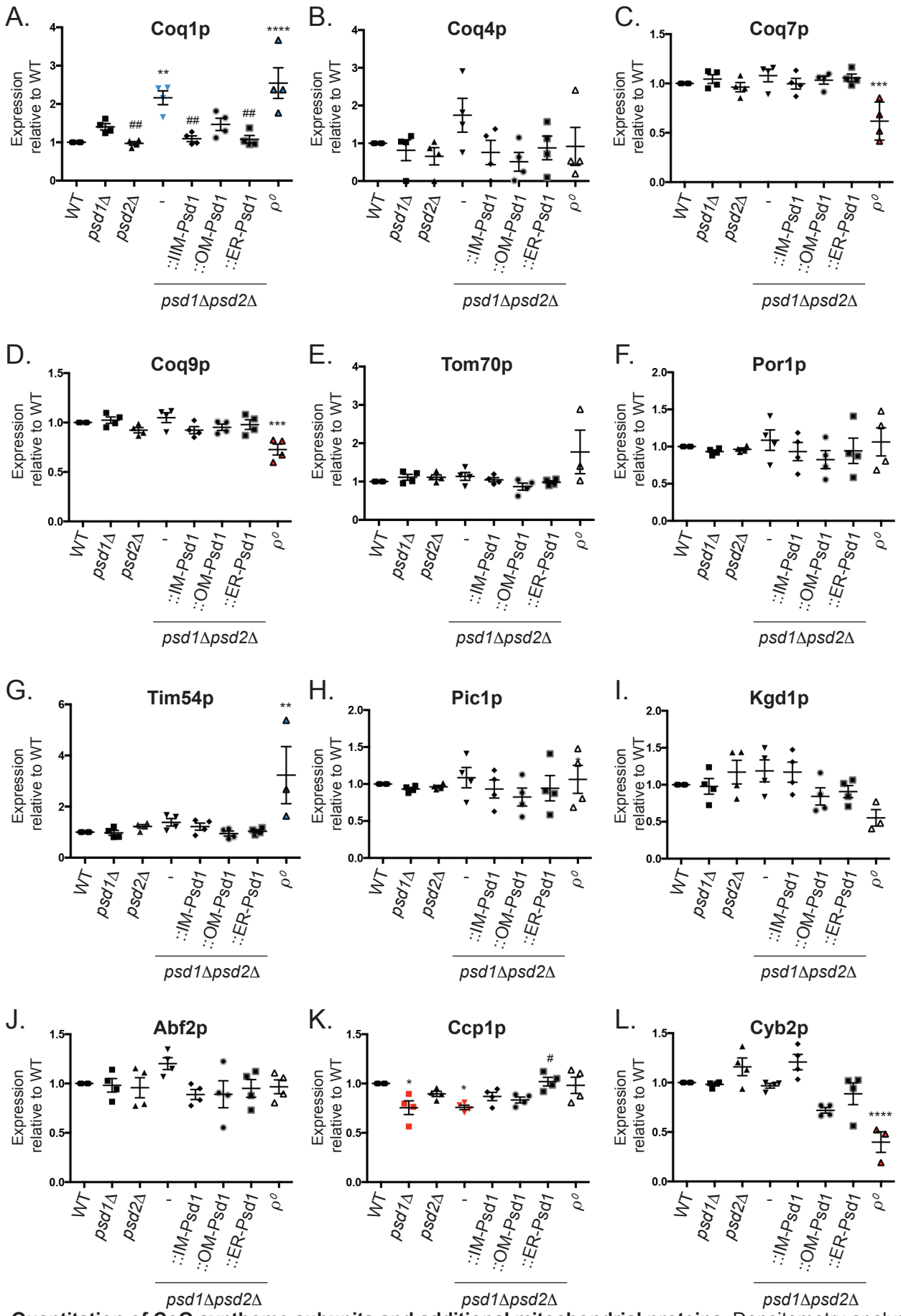

Fig S5. Quantitation of CoQ synthome subunits and additional mitochondrial proteins. Densitometry analysis of steady state protein amounts in isolated mitochondria (30 μg) from the indicated strains (representative immunoblots shown in Figure 5F). Analysis *versus*WT (*) or *psd1*Δ*psd2*Δ (#) was performed by one-way ANOVA ± S.E.M. for n=4.

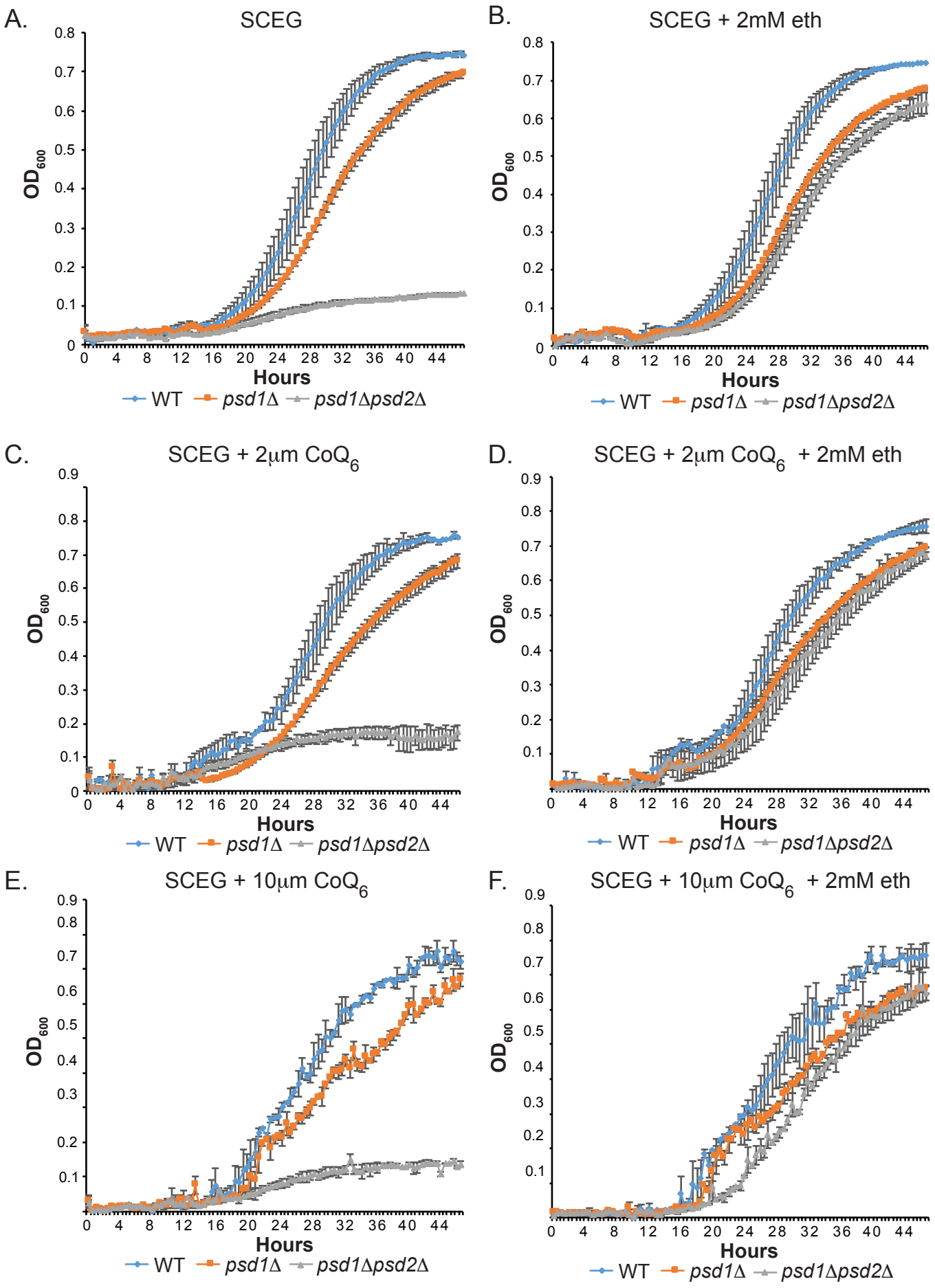
A.
SCEG
B.
SCEG + 2mM eth
C.
SCEG + 2μm CoQ6
D.
SCEG + 2μm CoQ6 + 2mM eth
E.
SCEG + 10μm CoQ6
F.
SCEG + 10μm CoQ6 + 2mM eth
OD600
Hours
WT
psd1Δ
psd1Δpsd2Δ

Fig S6

Fig S6. CoQ_6 supplementation does not rescue the *psd1*Δ and *psd1*Δ*psd2*Δ growth defects on respiratory medium. OD_{600} measurements were recorded every 30 minutes for a period of 48 hours at 30°C for yeast grown in (A) SCEG, (B) SCEG + 2mM ethanolamine (eth), (C) SCEG + 2μM CoQ6, (D) SCEG + 2μM CoQ6 + 2mM ethanolamine, (E) SCEG + 10μM CoQ6, and (F) SCEG + 10μM CoQ6 + 2mM ethanolamine. ± S.E.M. for n=2.